②

# NAVAL POSTGRADUATE SCHOOL
## Monterey, California

DTIC
SELECTED
NOV 2 0 1987
D

# THESIS

F-LAYER POLAR CAP ARCS

by

Denise D. Fite

September 1987

Thesis Advisor:                    S. Gnanalingam

8

*A186 849*

# REPORT DOCUMENTATION PAGE

| 1a REPORT SECURITY CLASSIFICATION | 1b RESTRICTIVE MARKINGS |
|---|---|
| Unclassified | |

| 2a SECURITY CLASSIFICATION AUTHORITY | 3 DISTRIBUTION/AVAILABILITY OF REPORT |
|---|---|
| 2b DECLASSIFICATION/DOWNGRADING SCHEDULE | Approved for public release; distribution is unlimited |

| 4 PERFORMING ORGANIZATION REPORT NUMBER(S) | 5 MONITORING ORGANIZATION REPORT NUMBER(S) |
|---|---|
| | |

| 6a NAME OF PERFORMING ORGANIZATION | 6b OFFICE SYMBOL (If applicable) | 7a NAME OF MONITORING ORGANIZATION |
|---|---|---|
| Naval Postgraduate School | 61 | Naval Postgraduate School |

| 6c ADDRESS (City, State, and ZIP Code) | 7b ADDRESS (City, State, and ZIP Code) |
|---|---|
| Monterey, California, 93943-5000 | Monterey, California, 93943-5000 |

| 8a NAME OF FUNDING/SPONSORING ORGANIZATION | 8b OFFICE SYMBOL (If applicable) | 9 PROCUREMENT INSTRUMENT IDENTIFICATION NUMBER |
|---|---|---|
| | | |

| 8c ADDRESS (City, State and ZIP Code) | 10 SOURCE OF FUNDING NUMBERS | | | |
|---|---|---|---|---|
| | PROGRAM ELEMENT NO | PROJECT NO | TASK NO | WORK UNIT ACCESSION NO |
| | | | | |

11 TITLE (Include Security Classification)

F-LAYER POLAR CAP ARCS

12 PERSONAL AUTHOR(S)

Fite, Denise D.

| 13a TYPE OF REPORT | 13b TIME COVERED | 14 DATE OF REPORT (Year Month Day) | 15 PAGE COUNT |
|---|---|---|---|
| Master's Thesis | FROM ___ TO ___ | 1987 September | 58 |

16 SUPPLEMENTARY NOTATION

| 17 | COSATI CODES | | 18 SUBJECT TERMS (Continue on reverse if necessary and identify by block number) |
|---|---|---|---|
| FIELD | GROUP | SUB-GROUP | Ionosphere; Polar caps; Ionospheric irregularities; C3I systems; polar cap arcs |
| | | | |
| | | | |

19 ABSTRACT (Continue on reverse if necessary and identify by block number)

Two types of ionospheric anomalies have been discovered recently in the polar cap: arcs and patches. Polar cap arcs are the focus of this study, which seeks correlation between arcs and total electron content (TEC) enhancements and amplitude scintillation effects. Simultaneous optical and radio frequency measurements were taken at Thule AFB and Qanaaq, Greenland, using an All Sky Imaging Photometer (ASIP) and a specially equipped Global Positioning System (GPS) receiver. Arcs were discovered to produce significant, rapidly varying TEC increases, and small but measurable amplitude scintillation.

| 20 DISTRIBUTION/AVAILABILITY OF ABSTRACT | 21 ABSTRACT SECURITY CLASSIFICATION |
|---|---|
| ☒ UNCLASSIFIED/UNLIMITED ☐ SAME AS RPT ☐ DTIC USERS | Unclassified |
| 22a NAME OF RESPONSIBLE INDIVIDUAL | 22b TELEPHONE (Include Area Code) | 22c OFFICE SYMBOL |
| S. Gnanalingam | (408) 646-2185 | 61Gm |

DD FORM 1473, 84 MAR    83 APR edition may be used until exhausted    SECURITY CLASSIFICATION OF THIS PAGE
All other editions are obsolete

1

F-Layer Polar Cap Arcs

by

Denise Dillon Fite
Lieutenant, United States Navy
B.A., Hunter College, 1975

Submitted in partial fulfillment of the
requirements for the degree of

MASTER OF SCIENCE IN SYSTEMS TECHNOLOGY
(Space Systems Operations)

from the

NAVAL POSTGRADUATE SCHOOL
September 1987

Author: _____
Denise Dillon Fite

Approved by: _____
S. Gnanalingam, Thesis Advisor

_____
E.J. Weber, Second Reader

_____
Rudolf Panholzer, Chairman, Space Systems
Academic Group

_____
Gordon E. Schacher, Dean of
Science and Engineering

2

## ABSTRACT

Two types of ionospheric anomalies have been discovered recently in the polar cap: patches and arcs. Polar cap arcs are the focus of this study, which seeks correlation between arcs and total electron content (TEC) enhancements and amplitude scintillation effects. Simultaneous optical and radio frequency measurements were taken at Thule AFB and Qanaaq, Greenland, using an All-Sky Imaging Photometer (ASIP) and a specially equipped Global Positioning System (GPS) receiver. Arcs were discovered to produce significant, rapidly varying TEC increases, and small but measurable amplitude scintillation.

A-1

3

# TABLE OF CONTENTS

4

## ACKNOWLEDGMENT

5

# I.  INTRODUCTION AND OBJECTIVES

Current command, control, communications and intelligence ($C^3I$) systems operate over the entire electromagnetic spectrum, and the increasing criticality of these systems to Orders of Battle (OOBs) demands an increased appreciation of the effects of the ionosphere on electromagnetic signals. Additionally, there is growing awareness that attention should be focussed, not only on the well-covered and well-understood middle latitudes, but also on potential conflict areas in the high latitudes, such as the so-called Greenland-Iceland-United Kingdom (G-I-UK) Gap and the Northern Pacific.  Unfortunately, the high latitude ionosphere (>65°) is probably the most complex, and in the polar cap in particular, the least understood and least studied of the ionospheric domains.  Recent discoveries of anomalies in the polar cap, as well as the growing sophistication and availability of data collection techniques, has contributed to a surge of interest in the high latitude ionosphere.

Of particular interest are the anomalies known as polar cap arcs.  Previous studies of the arcs have identified their structure and dynamics (Weber and Buchau, 1981); energy characteristics of the electron population (Hardy, 1984); Interplanetary Magnetic Field (IMF) dependency

6

(Gussenhoven,1982); and various characteristics of the magnetosphere-ionosphere coupling processes related to the arcs.

The Air Force Geophysics Laboratory (AFGL), among others, is conducting ongoing investigations in an effort to understand and characterize the high latitude ionosphere. Data analyzed in this thesis was collected from the AFGL stations in Thule Air Base and Qanaaq, Greenland, during the months of January and February, 1985. The data features recordings of high elevation angle satellite signals and photometer images taken simultaneously. The intent of the analysis in this thesis is to discover if the appearance of polar cap arcs is associated with any changes in the total electron content (TEC) or any amplitude scintillation problems in the satellite signal.

## II. <u>BACKGROUND</u>

The relationship between the ionosphere and electro-magnetic radiation is a particularly intimate one: solar radiation in the extreme ultraviolet (EUV) and X-ray range creates and maintains the ionosphere, while earth-based radio frequency (RF) radiation determined its existence, studies it and uses it as a vital transmission medium.

Although the existence of an electrically conducting layer of the atmosphere had been postulated earlier, confirmatory evidence became possible only with the development of radio, beginning around the turn of the century. Since then, RF has provided an important means of studying the ionosphere, beginning with the relatively simple, but effective and still widely employed, technique of using the high frequency (HF) band (~2-30 MHZ) for vertical sounding to determine the boundaries of the ionosphere. Increasingly sophisticated techniques are associated with progressively higher bands. For example, incoherent scatter radar, used to determine electron temperature and density, employs the very high frequency (VHF) and ultra high frequency (UHF) bands (~30-300 MHz and ~300 MHz-3 GHz); and the analysis of perturbations of satellite signals in the upper end of the UHF range (L-band microwave) is used to determine total electron content.

8

## A. MORPHOLOGY OF THE IONOSPHERE

The ionosphere is a blanket of stratified, partially ionized plasma surrounding the earth at an altitude of ~50-1000˙ kilometers. Ionospheric behavior is governed by processes which result in the production/destruction and transport of ionization; different mechanisms dominate according to both altitude and latitude. "Layering" into the D, E, F1 and F2 regions occurs because (a) the ionizing energy of solar radiation--a production mechanism--is deposited according to the absorption characteristics of the atmospheric constituents; (b) recombination--a destruction mechanism--depends on atmospheric density; and (c) the composition of the atmosphere changes with altitude, and prevailing types of production and loss, as well as transport, mechanisms are tied to these changes in composition. Prevailing mechanisms also change with respect to the geomagnetic latitude, reflecting the influence of the earth's magnetic field.

## B. PRODUCTION AND LOSS IN THE D, E, AND F1 REGIONS

The principal production process in the lower and middle ionosphere at low and middle latitudes ($\leq 65°$) is photo-ionization. Photo-ionization occurs when energy from solar EUV and X-ray photons is absorbed by atmospheric constituents, resulting in the creation of ion-electron pairs. Since both the density and composition of the

9

atmosphere change with altitude, different constituents are ionized by different wavelengths and energies of radiation.

The D region (~50-90 km) is characterized by positive ions of nitric oxide (NO$^+$) and molecular oxygen (O2$^+$), with Lyman $\alpha$ and hard X-rays being the main solar source of ionizing radiation. Molecular nitrogen (N2) is also ionized in significant amounts, but is rapidly converted to O2$^+$.

The E region (~90-140 km) is characterized by O2$^+$ and NO+, with some contribution from N2$^+$ and atomic oxygen (O$^+$). The solar radiation bands responsible are chiefly Lyman $\beta$, the Lyman continuum, Carbon III, and soft X-rays.

In the F region (>140 km), O$^+$ is the predominant ion, but also present are O2$^+$, N2$^+$, He$^+$, and N$^+$. The Lyman continuum and radiation at <800 Å are the principal sources of ionizing energy.

Photo-ionization is still the more prolific ion producing process at high latitudes, but in this instance, corpuscular ionization makes a significant contribution to the ion population, particularly at night, when it is the only source of ionization. Corpuscular ionization results from the interaction (i.e., collisions) of precipitating charged particles and the atmospheric constituents. Particle precipitation occurs toward the geomagnetic poles, where the geomagnetic field lines are closest to vertical.

The "destruction" of ionization--loss mechanisms--differ particularly with altitude. In the D region, the lowest and

10

most dense, a number of processes seem to be operative. Of these, the most important are believed to be dissociatve recombination of electrons with hydrated water cluster ions and photodetachment. Loss processes in the E and F1 region are better known and are clearly dominated by dissociatve recombination of $O2^.$ and $NO^.$. Table 1 summarizes the characteristics of the layers (Chamberlain, 1978, p.165).

## C. THE F2 LAYER

The F2 is the highest of the distinguishable ionospheric regions. The dominant production process is still photo-ionization. Because the region is optically thin, attenuation is not a factor as in the lower regions, and the ionization rate of the constituents is proportional to their number densities. In the F2 layer, the major constituent ionized is O, with a relatively small contribution from O2.

Above a certain altitude, known as the F2 peak, neutral density is low enough--and with electron density decreasing --that plasma diffusion processes, rather than photochemical loss mechanisms characterize the behavior of the region. In the lower F2 layer, below the F2 peak, both electron and neutral densities are high enough to provide a basis for photochemical loss mechanisms.

The controlling loss process is the very rapid ion-atom or ion-molecule charge exchange reaction (which converts $O^.$

11

TABLE 1.  CHARACTERISTICS OF IONOSPHERIC LAYERS

| Region | Nominal height of layer peak (km) | $N$ (max) (cm$^{-3}$) | $\alpha_{eff}$ (cm$^3$/sec) | Ion production | Recombination |
|---|---|---|---|---|---|
| D | 90 Lower following solar flare | $1.5 \times 10^4$ (noon); absent at night | $3 \times 10^{-8}$ | Ionization by solar X-rays, or Ly $\alpha$ ionization of NO. Enhanced ionization following solar flares due to X-ray ionization of all species. Electron attachment to O and $O_2$ forms negative ions; ratio of negative ions to electrons increases with depth and at night. | Electrons form negative ions, which are destroyed by photodetachment (daytime only), associative detachment ($O + O^- \rightarrow O_2 + e$), and mutual neutralization ($O^- + X^+ \rightarrow O + X$). |
| E | 110 | $1.5 \times 10^5$ (noon); $< 1 \times 10^4$ (night) | $10^{-8}$ | Ionization of $O_2$ may occur directly by absorption in the first ionization continuum ($h\nu > 12.0$ eV) Coronal X-rays also contribute, ionizing O, $O_2$, and $N_2$. Nighttime E and sporadic E (thin patches of extra ionization) are due to electron and meteor bombardment. Some E, radio reflections may be due to turbulence in normal E layer. | Dissociative recombination $O_2^+ + e \rightarrow O + O$ and $NO^+ + e \rightarrow N + O$. |
| F1 | 200 | $2.5 \times 10^5$ (noon); absent at night | $7 \times 10^{-9}$ | Ionization of O by Lyman "continuum" or by emission lines of He. This ionization probably accompanied by $N_2$ ionization, which disappears rapidly after sunset. | $O^+$ ions readily transfer charge to NO and perhaps to $O_2$. Most of the ionization is thus in molecular form and disappears by dissociative recombination. |
| F2 | 300 Height and electron density highly variable. Large daily, seasonal, and sunspot-cycle variations are combined with general erratic behavior. | $10^6$ (noon) $10^5$ (midnight) | $10^{-10} - 10^{-9}$ Variable; probably decreases with increasing height. | Ionization of O by same process producing F1; F2 formed because $\alpha_{eff}$ decreases with increasing height. F2 region produces little attenuation of radiation. Additional ionization processes may contribute in F2 that are attenuated in F1. | Recombination of molecular ions as in F1, but limiting process is here charge transfer, giving an attachment-like recombination law. |

12

to NO' and O2'), followed by dissociative recombination. Because the rate of the reaction is constrained by the neutral density, which decreases with altitude, the occurrence of the loss process decreases exponentially with height, and electron density continues to increase beyond the altitude of peak production.

After a certain height, the plasma diffusion rate becomes more rapid than the photochemical loss rate, and dominates the upper F2 layer, causing the electron density to decrease with height.

The F2 peak is the height at which the electron density is highest. It is a result of the net effect of the loss process and the plasma diffusion process. The peak occurs at the level where the time constants for the plasma diffusion and photochemical loss rates are approximately equal. (Gnanalingam, 1987)

D. THE HIGH LATITUDE IONOSPHERE

The high latitude plasma population is primarily governed by solar EUV ionization and precipitating electrons, as well as horizontal and magnetic field aligned transport processes.

The solar EUV component varies smoothly. However, because the magnetosphere-ionosphere (M-I) coupling processes are both dynamic and interactive, electron precipitation throughout the high latitude ionosphere varies

13

greatly in energy distribution and with latitude and local time. Field aligned currents, electric fields and charged particles represent the principal coupling mechanisms between the magnetosphere and the ionosphere. Electric fields are responsible for the large scale plasma convection patterns that are characteristic of the high latitude regions. Charged particles, precipitating along magnetic field lines from the magnetosphere, are believed to be the source of the upward field aligned currents, which are also associated with gradients in the electric fields. The particles may also be accelerated; they typically have a higher range of energies than that of their solar wind/magnetosheath source region. This results in not only horizontal and vertical plasma structures but also a source of free energy for the plasma instability processes characteristic of the region.

The major domains of the high latitude ionosphere--the auroral zone and the polar cap--are generally identified by both geomagnetic latitude and characteristic phenomena. They differ in magnetic field topology, convective electric field patterns and particle precipitation characteristics.

The auroral zone encompasses the region from ~60°-75° Corrected Geomagnetic Latitude (CGL). The magnetic field lines are, for the most part, closed, and the source of the precipitating electrons is the magnetosphere's plasma sheet: the central plasma sheet (CPS) for the equatorward portion,

14

with particle energies up to a few kilo electron volts (keV); and the boundary plasma sheet (BPS) for the poleward portion, with particle energies up to a few hundred eV. The large scale electric fields are set up to support sunward convection, except in the Harang discontinuity region near midnight and the dayside cusp near noon.

The polar cap is the poleward region bounded by the instantaneous auroral oval. Magnetic field lines are open, or close at such great distances down the magnetotail that they may be treated as open. Polar electron precipitation is believed to originate directly from the magnetosheath, and is customarily classed by energy level. Polar rain has typical energies of ~100 eV and is uniformly distributed over large areas. Polar showers have mean energies of ~1 keV, and are enhanced flux areas embedded in larger regions of polar rain. Polar squalls are localized zones of intense precipitation, with particle energies of up to several keV. The polar cap is generally an area of anti-sunward convection. (Burke, 1982, pp.685-686; Heelis, 1982, p.567)
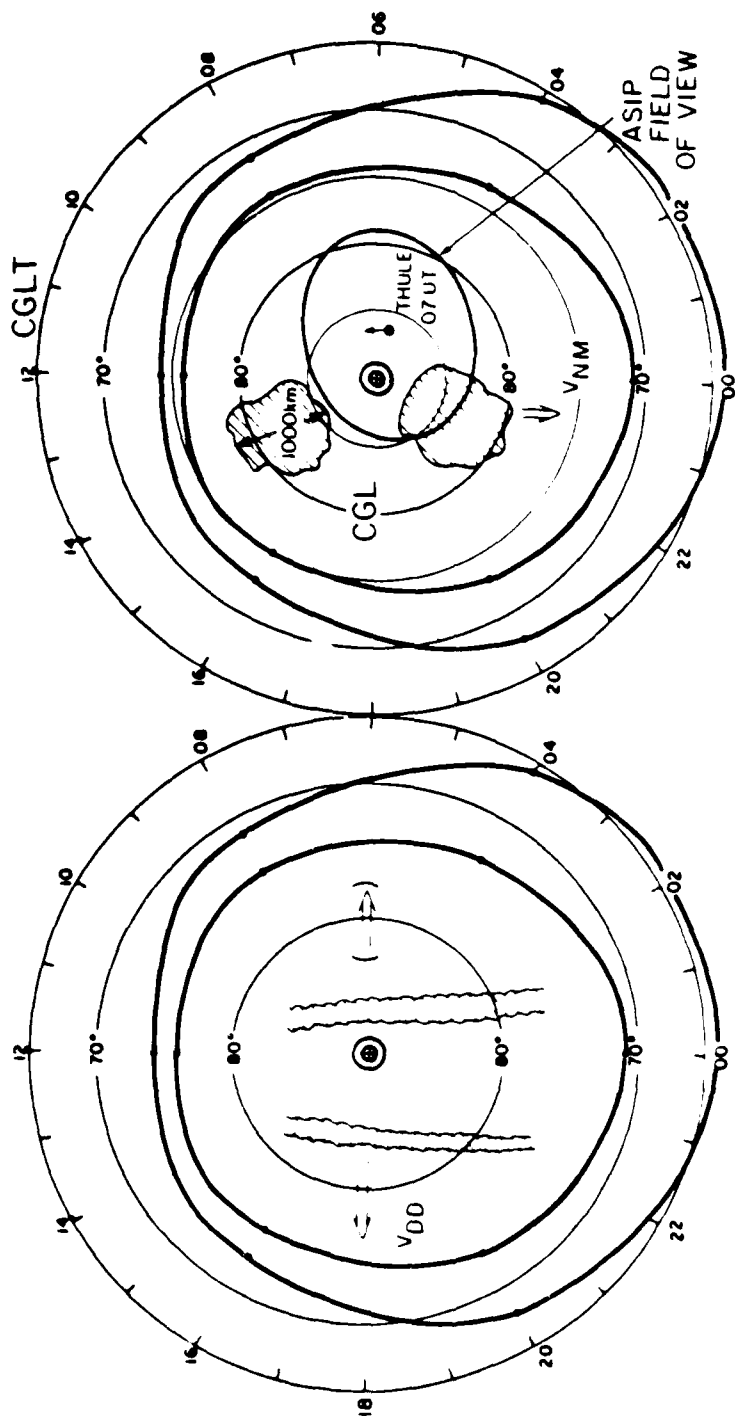
E. POLAR CAP IRREGULARITIES

The high latitude F layer is riddled with irregularities which have a broad range of scale sizes (from $10^{-2} - 10^{5}$ m) and a global distribution. Interest in the high latitude ionospheric domain has lately begun to focus on the heretofore neglected polar cap as well as the more obviously

15

dynamic auroral zone. Recently recognized irregularities in the polar cap illustrate both particle precipitation and the convective transport processes that dominate the region.

F-layer patches are regions of enhanced ionization produced in the dayside ionosphere, which are then transported into and across the polar cap and ultimately into the nightside auroral oval (Figure 1b). The patches are characterized by airglow emission at 6300 Å; high electron density (5-10 times background level); large size (~1000km in horizontal extent); and speeds of up to 1000 m/sec in an anti-sunward direction. The patches also have an IMF dependency, occurring when the IMF has a southerly component (i.e., $B_z < 0$) and when the geomagnetic field is moderately disturbed. As these patches move through the ionosphere, they cause significant increases in the ambient TEC and measurable amplitude scintillation in both UHF and L-band satellite signals through which they pass. (Weber et al., 1986, p.12121)

A second recently recognized phenomenon is the polar cap arc (Figure 2). The arcs tend to appear during magnetically quiet periods, and when the IMF has a northerly component (i.e., $B_z > 0$). They are nominally sun-aligned, and drift in a direction perpendicular to their alignment, that is, dawn-to-dusk (Figure 1a). They have a curtain-like structure: height and length are large relative to width. They stretch

16

TYPE 1 SUNALIGNED ARCS
DAWN-DUSK DRIFT (PREDOMINANT)

TYPE 2 PATCHES
ANTI-SUNWARD DRIFT

POLAR CAP F REGION STRUCTURES

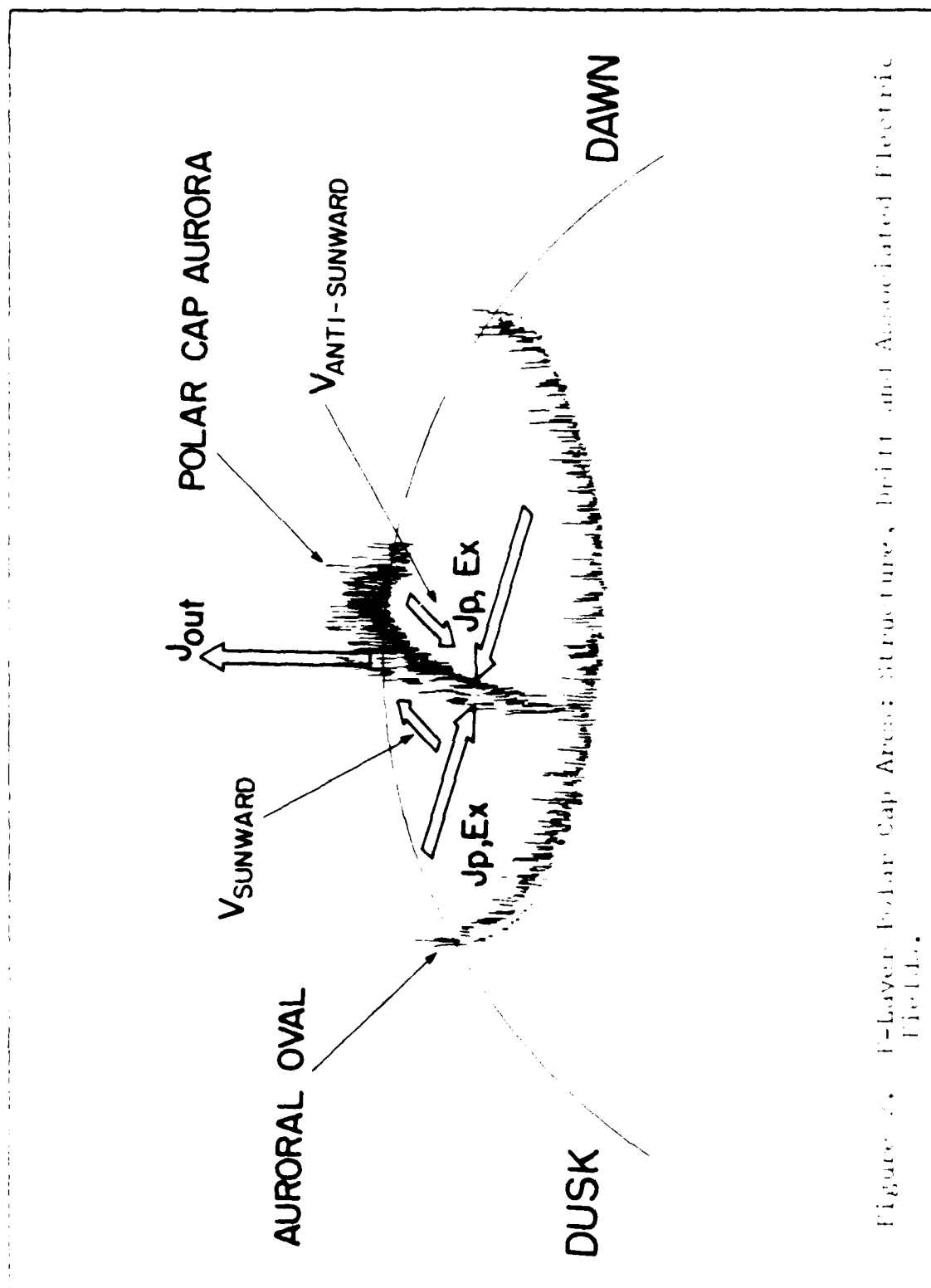Figure 1(a) and (b). Irregularities of the Polar Cap F-Layer: Arcs and Patches

17

Figure .. F-Layer Polar Cap Arcs: Structure, Drift and Associated Electric Field.

18

from an altitude of ~250km to ~1000 km. As in the patches, the arcs have an optical signature at 6300 Å, and are associated with upward field aligned currents. (Akasofu, 1985, pp.15-18; Weber and Buchau, 1981, p.125; Carlson et al., 1984, p.895 and p.898)


## F. DESCRIPTION OF THE EXPERIMENT

Data used in this thesis was collected at the AFGL stations at Thule and Qanaaq, Greenland. The instruments used were an All Sky Imaging Photometer (ASIP), at Qanaaq, and a specially equipped Global Positioning System (GPS) satellite receiver at Thule. Thule is located at 76'32'N, 68'42'W, and Qanaaq at 77'28'N, 69'13'W (geographic coordinates). Their great circle separation is 104.5 km, and the true azimuth angle from Qanaaq to Thule is 179'39'. Although the ASIP and the GPS receiver are not collocated, their spatial separation is not considered significant relative to the large area covered by the ASIP (Figure 3).

Polar cap arcs are believed to be caused by precipitating soft electrons, and would therefore represent regions of increased electron density and TEC. Ionospheric sounders are the most common means for remotely determining electron density. However, the arcs cause spread F on sounder data, making it extremely difficult to extract correct critical frequency and thus determine electron density. An entirely different technique is used in the
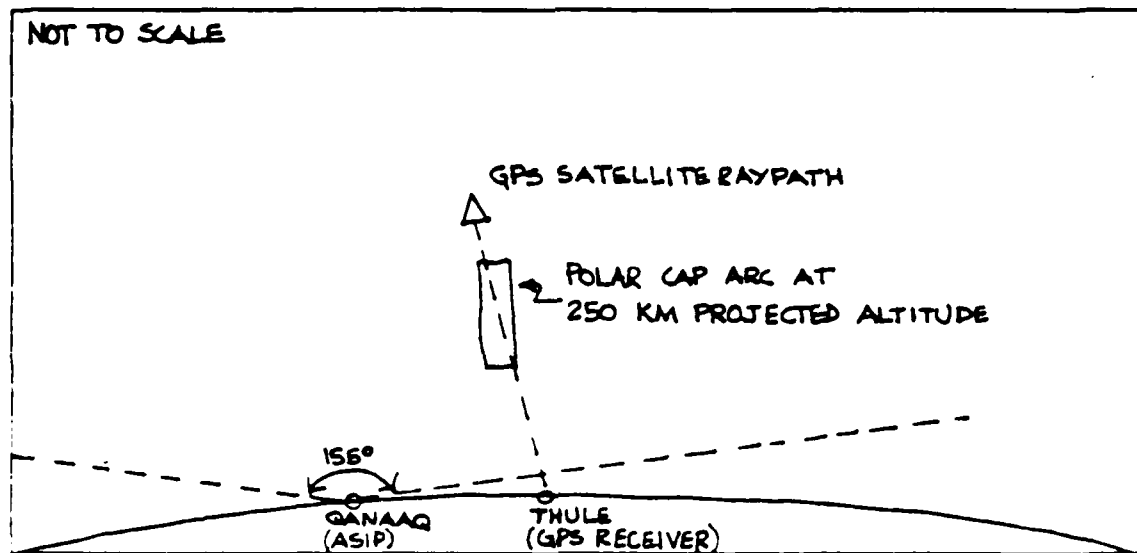
19

Figure 3. Geometry of GPS receiver and ASIP locations.

collection of GPS data, and using the GPS data allows unambiguous determination of TEC.

The spread F masking in the ionogram indicates the presence of structured irregularities in the arcs. Irregularities also cause amplitude scintillation, and the occurrence of changes in scintillation indices caused by the arcs are further indication of the presence of irregularities. The GPS data includes amplitude scintillation measurements, taken simultaneously with the TEC measurements, and allows further definition of the arcs and the irregularities they contain.

At the time the images and satellite receiver recording were made (January and February), the Thule/Qanaaq area was undergoing 24 hour periods of darkness. Therefore, solar EUV was minimal. The ASIP is programmed to image

20

continuously under moonless conditions after the sun has reached a solar depression angle of 10°, and data from the satellite receiver is recorded continuously. Of the 5 GPS satellites currently operating, at least 1 was in view up to 4 hours at an elevation angle of greater than 20°, for a total of ~18 hours.

## G. THE ALL SKY IMAGING PHOTOMETER

The ASIP is a monochromatic imaging system with high sensitivity (threshold = ~20 Rayleighs) developed for low light level research. An upward-looking, wide angle lens images a large section of the sky (155° field of view) onto an interference filter near the focal plane. The optics are telecentric in design, ensuring the same size light cone at the focal plane for each point in the field of view, and allowing the use of narrowband interference filters (~25 Å). Although up to four filters can be mounted on a filter wheel to allow sequential measurements, only the 6300 Å OI and the 4278 Å N2⁺ were used at Qanaaq. The field is re-imaged onto the faceplate of a two stage image intensifier. The image is then coupled to a 35 mm Automax camera, using Kodak 4X film at ~10 seconds exposure.

Filters at 6300 Å and 4278 Å are used because those wavelengths tag the photochemical reactions of specific atoms and molecules which predominate at different heights in the ionosphere, and can therefore identify the altitudes

21

at which the phenomena occur. For example, arcs have been observed at both E and F region heights, and their presence can be optically verified because the filters monitor the following reactions:

soft particles ---> $e^{-***} + O$ --->$O^*$ ~~~> $h\nu$ 6300 Å

(which occurs at F region heights where the dominant atmospheric constituent is O), and

harder particles --> $e^{-***} + N2$ ---> $N2^*$ ~~~> $h\nu$ 4278 Å

(which occurs at E region heights where N2 is the dominant atmospheric constituent).

Control sequencing is provided by a programmable camera control system which controls the mechanical operation and camera exposure setting. Date, time and filter setting are automatically recorded on each image. The ASIP also has a light sensor which will disable the camera under moonlit or sunlit conditions.

The ASIP is most often used to map the structure and dynamics of auroral and airglow structures rather than to measure quantitatively absolute intensities. In this case, the ASIP was used to verify the presence of an arc and to indicate its position in relation to the ray path of the satellite. (Weber et al., 1977,pp.7-9)

22

Figure 4 lists system specifications (Weber et al., 1977, p.11).

| | |
|---|---|
| Field of View: | $155^{\circ}$ |
| Pass Band: | 25 Å at f 1.4; 5 Å at f 8 |
| Resolution: | $1/2^{\circ}$ zenith, $2^{\circ}$ horizon |
| Spectral Response: | S - 20, exceeding 100 $\mu A$/lumen |
| Picture Storage: | No detectable degradation for up to 3 sec |
| Tube Gain: | Photon noise granularity visible above tube noise |
| Threshold Sensitivity: | 20 R at 2 sec exposure |
| Dynamic Range: | 20 R to 10 kR covered by 3 preset HV settings |
| Flatness of Field: | 30 percent loss at edge of field |
| Repetition Rate: | Typically 20 sec for complete filter cycle |

Figure 4.   Summary of ASIP specifications

## H.   THE GPS RECEIVER AND MEASUREMENT TECHNIQUES

The NAVSTAR Global Positioning System (GPS) is a satellite based navigation system which provides accurate 3-dimensional position and timing information to users.

The constellation, eventually planned to contain 18 satellites, currently has 5, at 63' inclination in 12 hour, sidereal-synchronous orbits.   The satellites broadcast continuously on 1.57542 GHz (L1) and 1.22760 GHz (L2). Their signals are coherently derived, biphase modulated at 10 MHz with a pseudo-random noise (PRN) code and contain ephemeris, satellite clock drift, signal code state and ionospheric propagation delay data.   The user's receiver measures the pseudo range (measured transit time of the signal multiplied by the speed of light) and pseudo range

rate , using the encoded signals from 4 satellites. These measurements can then be converted to a user 3-dimensional position and velocity. (Demaro, 1981, pp.36-37; Cretcher, 1975, pp.406-407)

The advantages of the GPS satellites for high latitude research lie in (a) their inclination, which allows high look angles for significant periods of time in the true polar regions, well above the cusp and the auroral oval, and (b) the system's 2 frequency design feature which allows the user to correct for signal delays due to ionospheric effects. (Demaro, 1981, pp.36-37; Cretcher, 1975, pp.406-407).

One of the critical ionospheric effects on radio wave propagation is the group delay of the modulation envelope of the wave. Other ionospheric effects, measurable by the 2 frequency design of the GPS system, are the differential carrier phase advance and amplitude and phase scintillation. The ionospheric parameter responsible for these effects is TEC, the total number of free electrons which the transmitted signal encounters in the ionosphere. The group delay and carrier phase advance are proportional, to the first order, to the TEC in the transionospheric path of the wave. (Klobuchar, 1983, pp.5 and 16)

24

## 1. Group delay

Group delay is the additional time delay of a signal transmitted from above the ionosphere, and is generally given by:

$$\Delta t = (40.3/cf^2) \times TEC$$

where $c$ is the speed of light, $f$ is the frequency of the wave, and TEC is in $el/m^2$.

For a system using a pair of fairly widely spaced frequencies, group delay as a function of frequency is:

$$\Delta t_1 = (k/cf_1^2) \times TEC \quad , \quad \Delta t_2 = (k/cf_2^2) \times TEC$$

where $t_1$ is the group delay at frequency $f_1$ and $t_2$ is the group delay at frequency $f_2$. If $f_1$ is the primary frequency and $f_2$ is the lower frequency chosen for correction of ionospherically induced errors, then:

$$\delta(\Delta t) = (k/c) \times TEC \, (1/f_2^2 - 1/f_1^2)$$
$$= \Delta t_1 \, (f_1^2 - f_2^2)/f_2^2$$

or

$$\Delta t_1 = (f_2^2/f_1^2 - f_2^2) \times \delta(\Delta t)$$

where $\delta(\Delta t)$ is the difference in the time delays measured simultaneously on the 2 frequencies, in nanoseconds.

With GPS, the user's receiver converts the received spectrum to equivalent carriers with 10.23 MHz modulation. The 10 MHz modulation is transmitted with a known phase difference on the 2 carriers, and the received modulation phase difference is a direct measurement of the

25

group delay. The group delay is related to the equivalent TEC by:

$$TEC = (2.852 \times 10^{16}) \times \delta(\Delta t)$$

To obtain the absolute TEC, one value of TEC is obtained to fix the relative phase advance scale to an absolute one throughout each satellite pass. Usually, several independent values of group delay are fitted on an r.m.s. basis to the continuous relative phase advance scale. (Klobuchar, 1983, pp.7-9; Klobuchar et al., 1985, p.2)

### 2. Differential carrier phase advance

In addition to group (or modulation) delay, the phase of the carrier is changed by the ionosphere, with the carrier phase being advanced with respect to its phase in the absence of an ionosphere. Carrier phase advance is related to TEC by:

$$\delta(\varphi) = (1.34 \times 10^{-7}/f) \times TEC$$

where f is the carrier frequency in Hertz.

The GPS satellites transmit 2 coherently derived carrier frequencies for the purpose of measuring differential carrier phase advance. For the GPS frequencies L1 (1.575 GHz) and L2 (1.228 GHz), the phase advance difference, referenced to the lower frequency, is:

$$\Delta(\delta\varphi) = (1.34 \times 10^{-7}/L2) \times (m^2 - 1/m^2) \times TEC$$

where m is L1/L2 for the GPS frequencies. For the GPS frequencies,

$$\Delta(\delta\varphi) = (4.31 \times 10^{-17}) \times TEC$$

26

or

$$TEC = (2.32 \times 10^{16} \ el/m^2) \ \triangle(\delta\varphi)$$

(per complete $2\pi$ cycle of differential carrier phase advance between L1 and L2, measured at L2).

Because the 2 coherent GPS carriers are relatively close, the measured ionospheric phase advance at L2 minus that at L1 is only 39% of the total phase advance at L2. Still, the technique has a sensitivity of better than 0.1 radians r.m.s. in a 16 Hz bandwidth using an omnidirectional antenna, and has the added advantage of removing contributions to the phase advance due to geometric Doppler changes. (Klobuchar, 1983, p.10; Klobuchar et al., 1985, p.2)

The differential carrier phase advance measurement accurately measures relative changes in TEC. Background TEC, however, generally produces much more than one complete cycle of carrier phase advance. Group delay is used, therefore, to measure absolute TEC.

3.  $\underline{S_4}$

The third parameter measured by the GPS receiver is amplitude scintillation, which is presented as changes in the $S_4$ index. The $S_4$ scintillation index is the normalized variance of signal intensity and is a widely used measure of signal fluctuations caused by ionospheric irregularities. (Yeh and Liu, 1982, p.324)

I. REDUCTION OF GPS DATA

All the GPS data were recorded on 5 channel magnetic tape and processed at AFGL using a computer program developed specifically for that purpose. The program unpacks and reformats the data for compatability with the AFGL CYBER computer, determines calibration levels for each channel, converts voltages to TEC units, and produces 3 output files for additional analysis. The first of these contains 6 second averages of group delay (absolute TEC). The second file contains $S_4$ values measured at L2 at 1 minute sliding averages. The third file contains deramped carrier phase advance values (relative TEC). (Doherty, 1987)

## III. METHODOLOGY OF THE EXPERIMENT

Data simultaneously recorded by the ASIP and the GPS receiver yielded four types of information: (a) 6300 $\AA$ optical images; (b) absolute TEC; (c) relative TEC; and (d) $S_4$. ASIP images were used to determine both the presence of the arcs and the periods when they crossed the raypath of the GPS receiver. Data from the GPS receiver were then examined to establish the degree of correlation, if any, between the presence of an arc and changes in the TEC levels and the $S_4$ index.

### A. ANALYSIS OF DATA

Comparison of data showed excellent correlation between the onset of an arc's passage through the GPS raypath (i.e., the arc's leading edge) and a relative increase in TEC. A total of 7 arcs from January and February 1985 were examined; 4 are represented here. For the instances examined, the average relative increase in TEC was ~3.6 units (1 unit = $10^{16}$ el/m$^2$), with the lowest increase at ~1.7 units and the greatest at ~5.0 units. In all but one of the instances, there was also a small but measurable change in the $S_4$ index: an average increase in $S_4$ from ~0.06 to ~0.1 ( $S_4$ = ~0.04). Further comparison showed, however, that the arcs followed different patterns of behavior, even

29

with respect to the clear association between onset of leading edge and TEC enhancement. Specific cases will be presented to illustrate some of the differing characteristics of the arcs.

1. Case 1: 26 January 1985

The primary arc of this event began encounter with the GPS signal at ~0804 UT on 26 January 1985, while still relatively unformed. The arc cohered in the raypath, and did not clear it until 0920 UT. The images (Figures 5 and 6) show the slow formation and stagnation of the arc and this is reflected in the clear cut but gradual increase in TEC. The peak relative increase in TEC was ~4.4 units, which occurred at 0822 UT, early in the arc's transit. The arc hovered in or near the raypath for over an hour, but the TEC levels, while remaining elevated, never reached the relative maximum achieved at 0822 UT. A plot of the relative TEC changes is at Figure 7.

In this instance, the end of encounter is also unmistakable. The arc had completely cleared the raypath by 0920 UT, and the relative TEC levels dropped abruptly. Although not shown here, the relative TEC levels continued undisturbed for some hours after the arc's passage.

Figure 8 is a plot of the relative TEC for the same 2½ period on the following day (0729 - 0947 UT, 27 January 1985), during which there were no arcs recorded or observed.
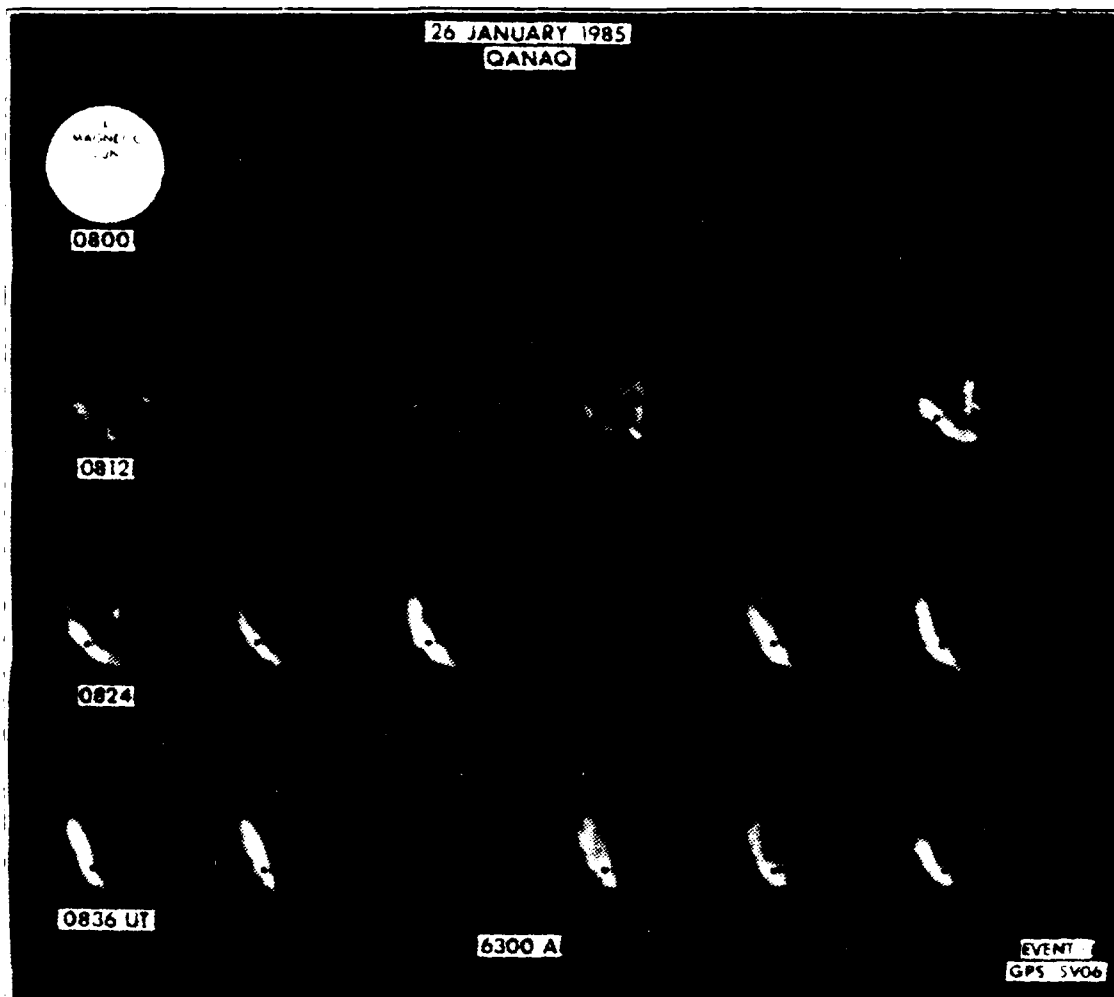
Figure 5.  ASIP Images: 0800 - 0846 UT, 26 January 1985.
The "Magnetic Sun" symbol marks the noon -
midnight meridian.  GPS raypath is indicated
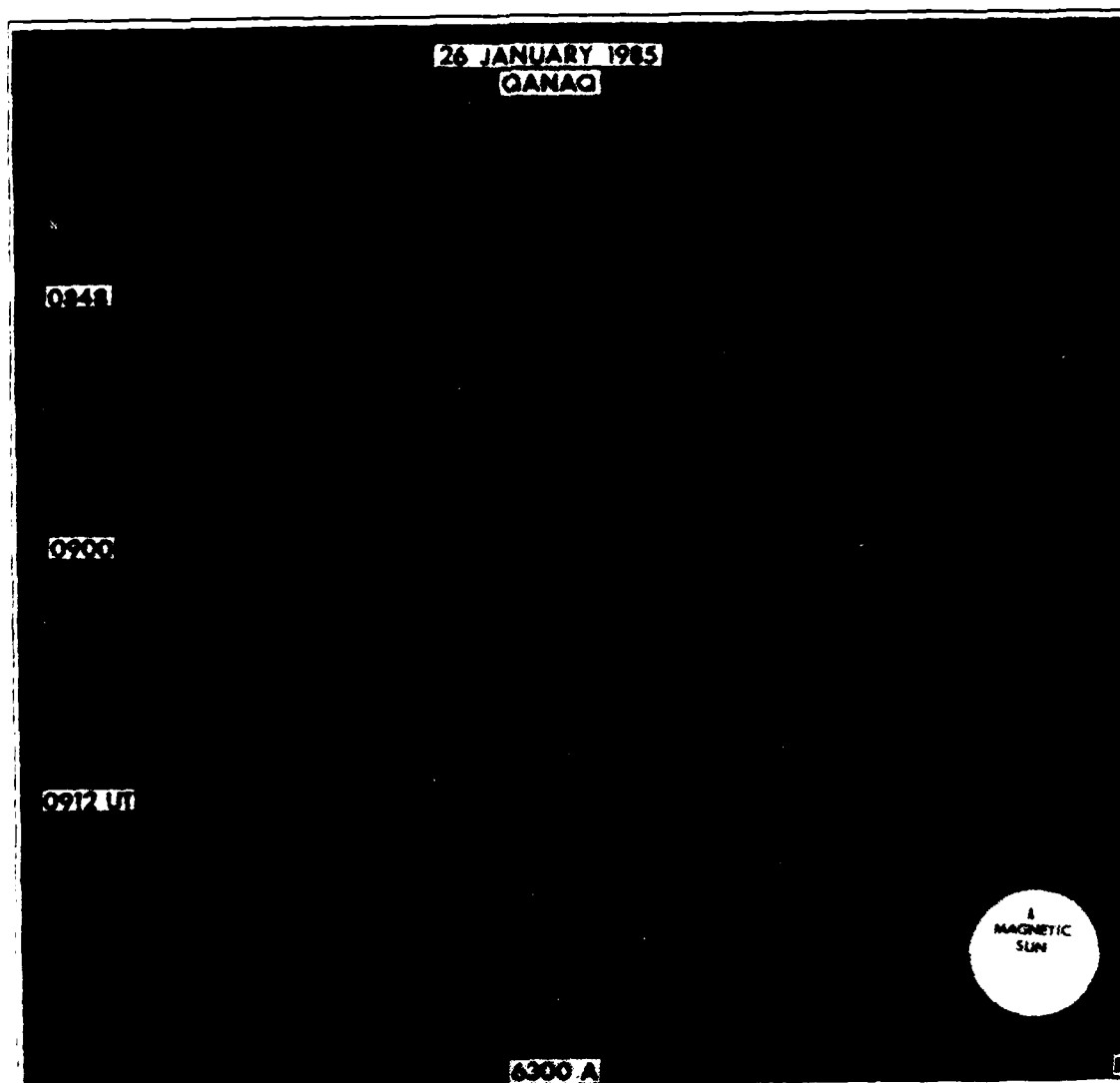by the black dot in each image.

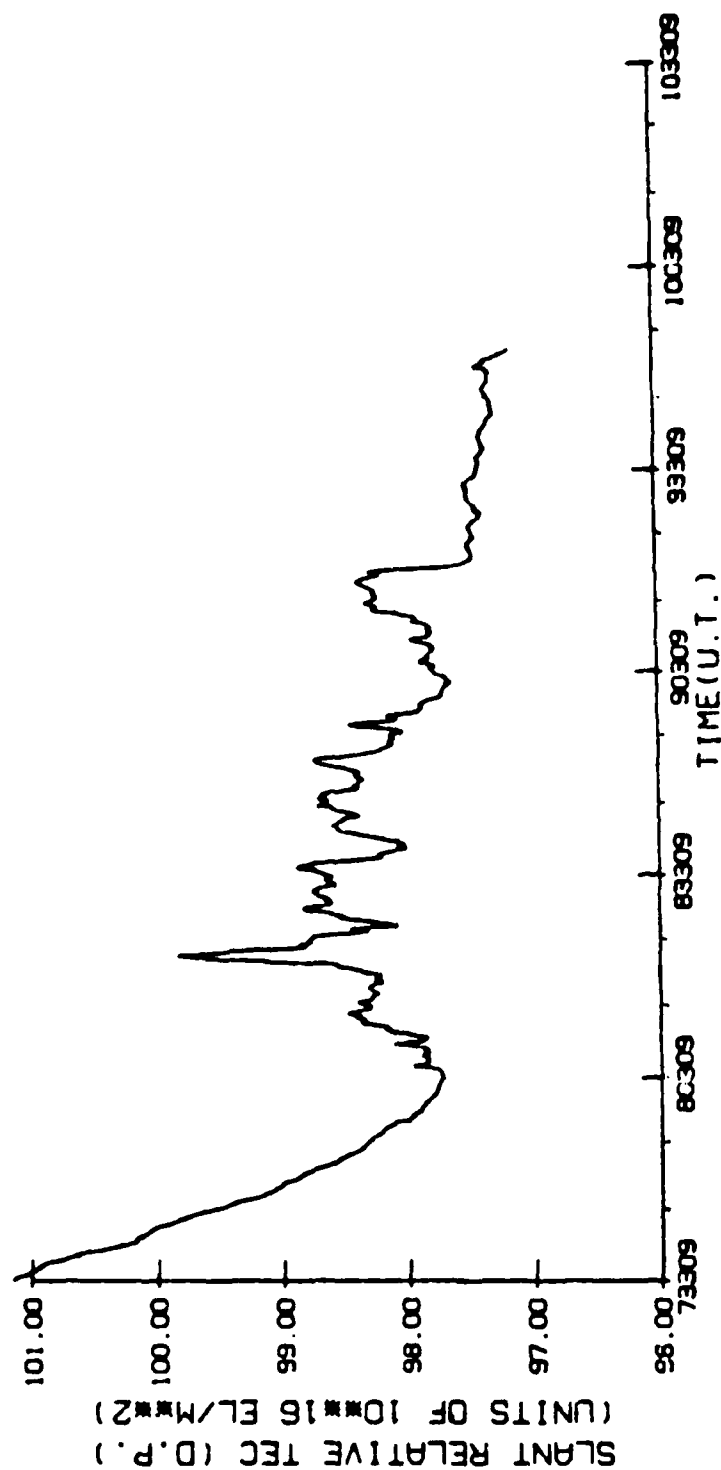Figure 6.   ASIP Images:  0848 - 0920 UT, 26 January 1985

32

Figure 7. Relative TEC for 26 January, 0800 – 0320 UT. Time on graph is in hours, minutes and seconds. Date is Julian date. Absolute TEC values were not calibrated for this observation period, and an arbitrary factor has been added to prevent negative values.
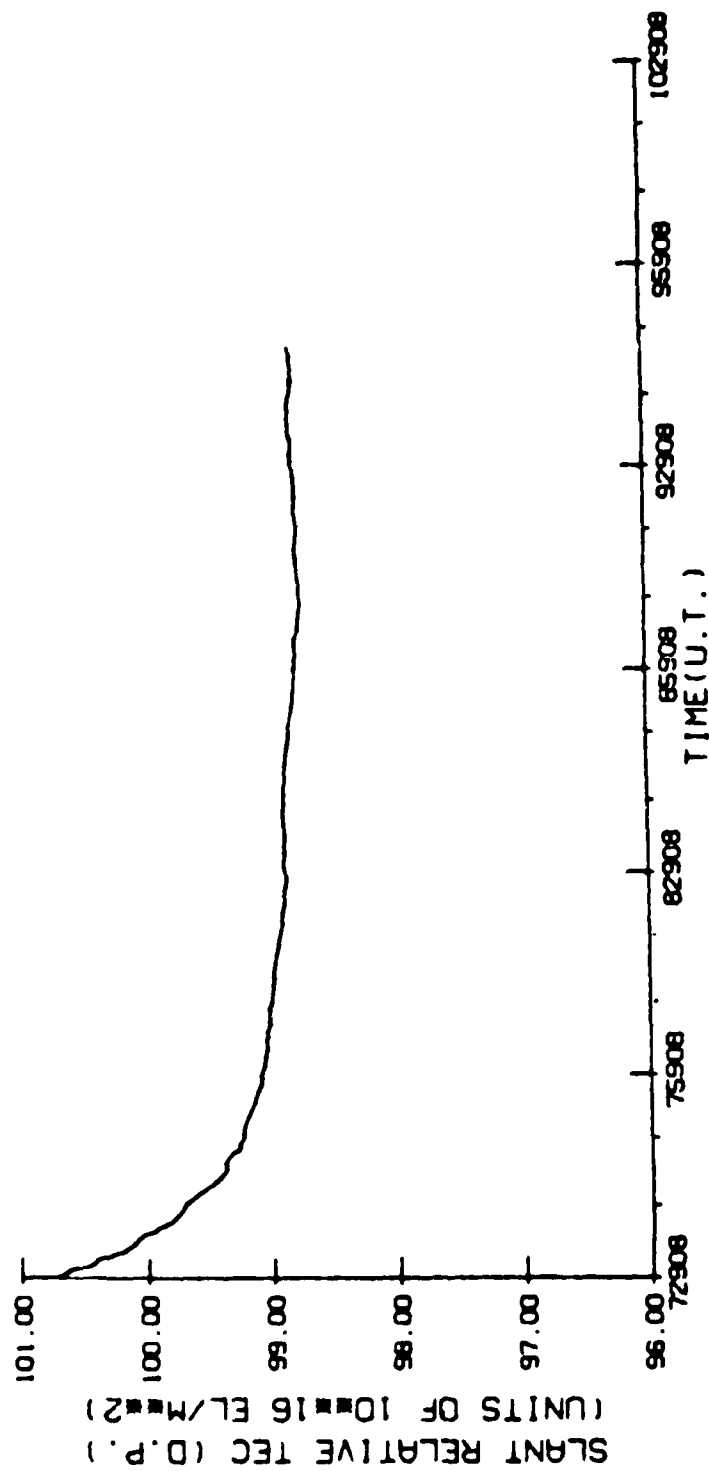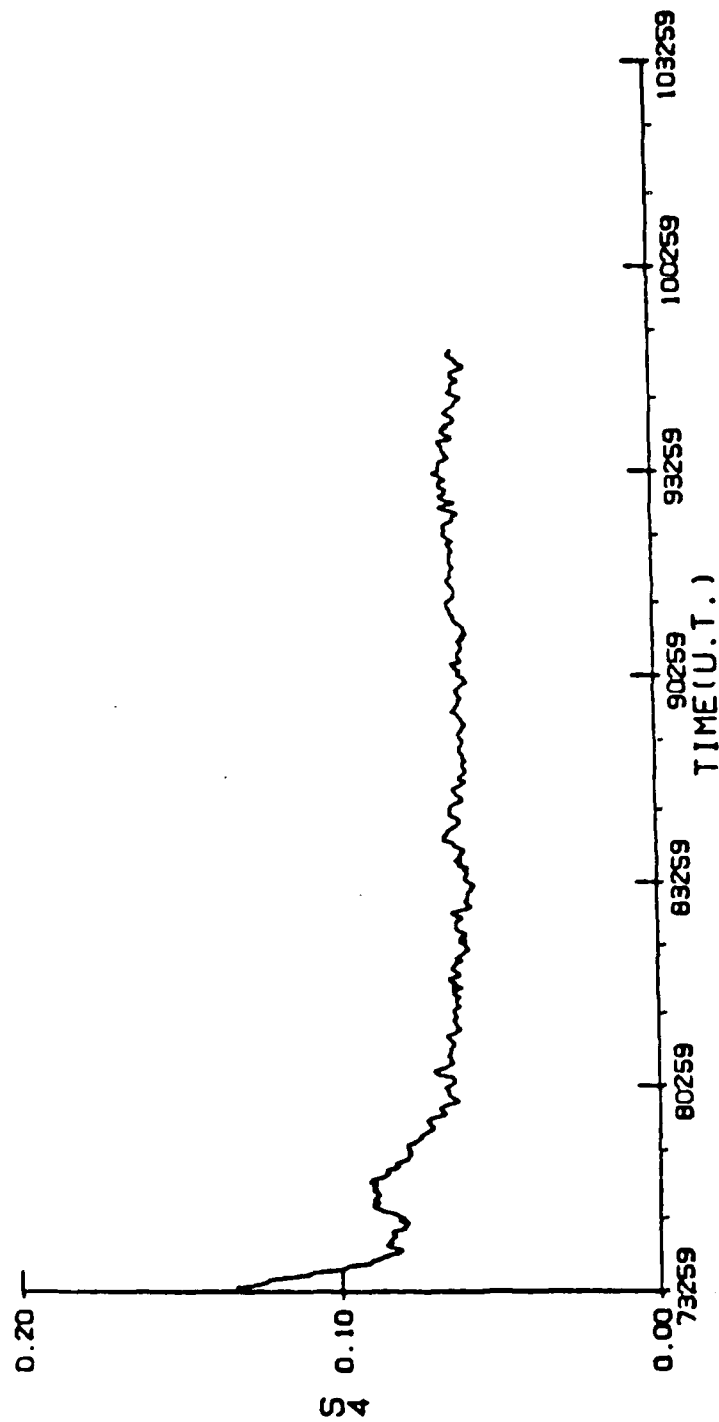
33

Figure 8. Relative TEC for 27 January, 0804 - 0920.

The GPS satellites repeat their orbits with only a four minute daily change in their rise and set times, so that Figures 7 and 8 represent data taken from the same satellite at very nearly the same times on subsequent days. Comparison of the TEC curves clearly reveals significant differences in the TEC behavior on the two days. During the passage of the arc on 26 January, the TEC variations are many, large and abrupt, reflecting the disturbed conditions generated by the arc. The 27 January plot shows only a very gradual and very small decrease from 0804 - 0920 UT, with no enhancements to mar the smoothness of the curve. Since this tallies with the fact that there were no arcs observed, this plot is illustrative of conditions unperturbed by the presence or passage of an arc.

The obvious increase in TEC was not, in this instance, coupled to any measurable change in S. (Figures 9 and 10).
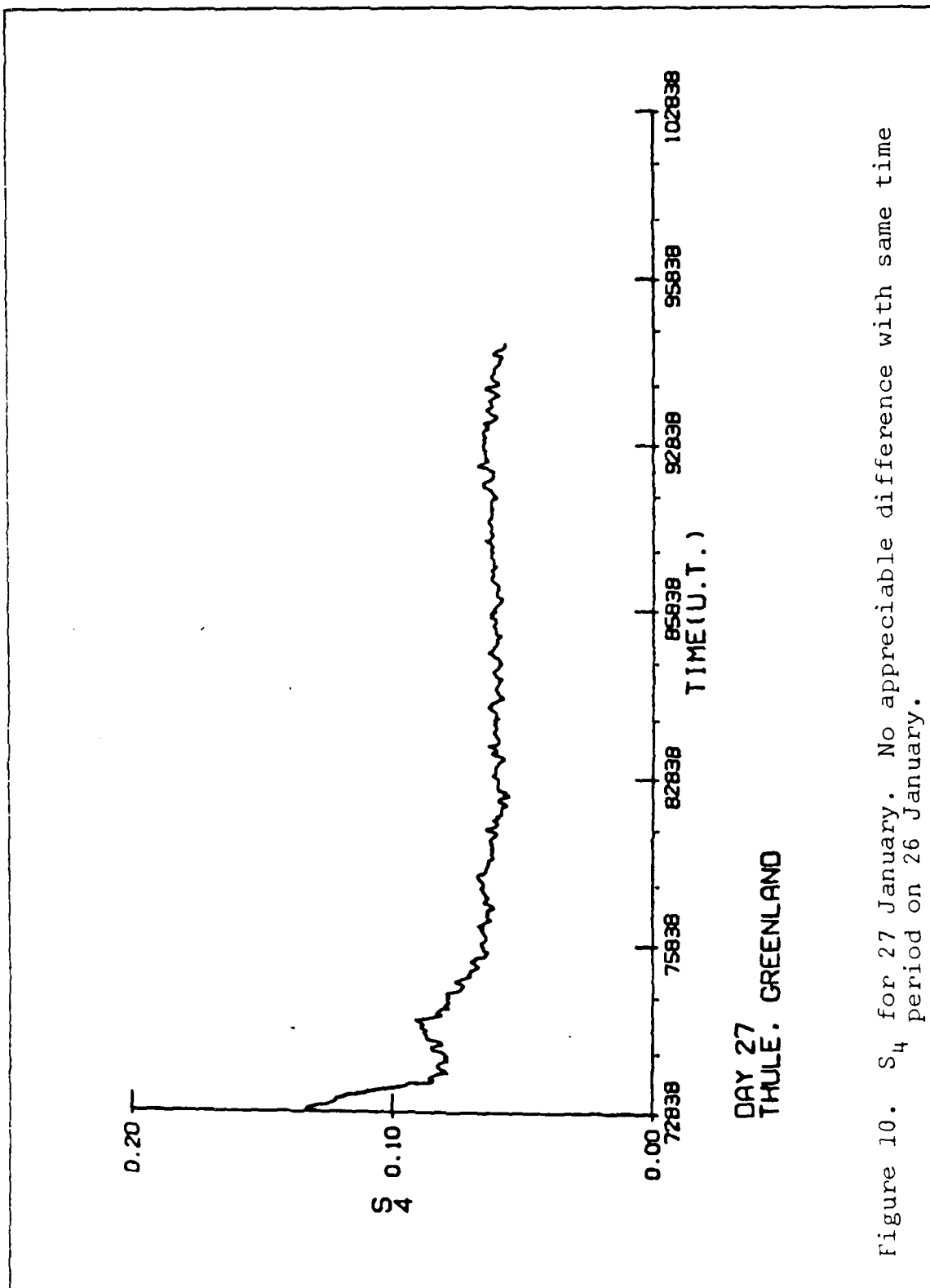
2.    Case 2: 16 February 1985

This arc also had distinct leading and trailing edges, but its transit was much faster than that of the arc just examined. It entered the raypath already well formed, at 1037 UT, 16 February, had traversed it completely and dissipated (out of the raypath) by 1053 UT. It has a less substantial appearance in the ASIP images (Figure 11), and maximum relative change in TEC was ~2.2 units (Figure 12).

35

DAY 26
THULE. GREENLAND

TIME(U.T.)

103259
100259
93259
90259
83259
80259
73259

0.20
0.10
0.00

S₄

Figure 9.  S₄ for 26 January, 0804- 0920 UT.

Figure 10. $S_4$ for 27 January. No appreciable difference with same time period on 26 January.
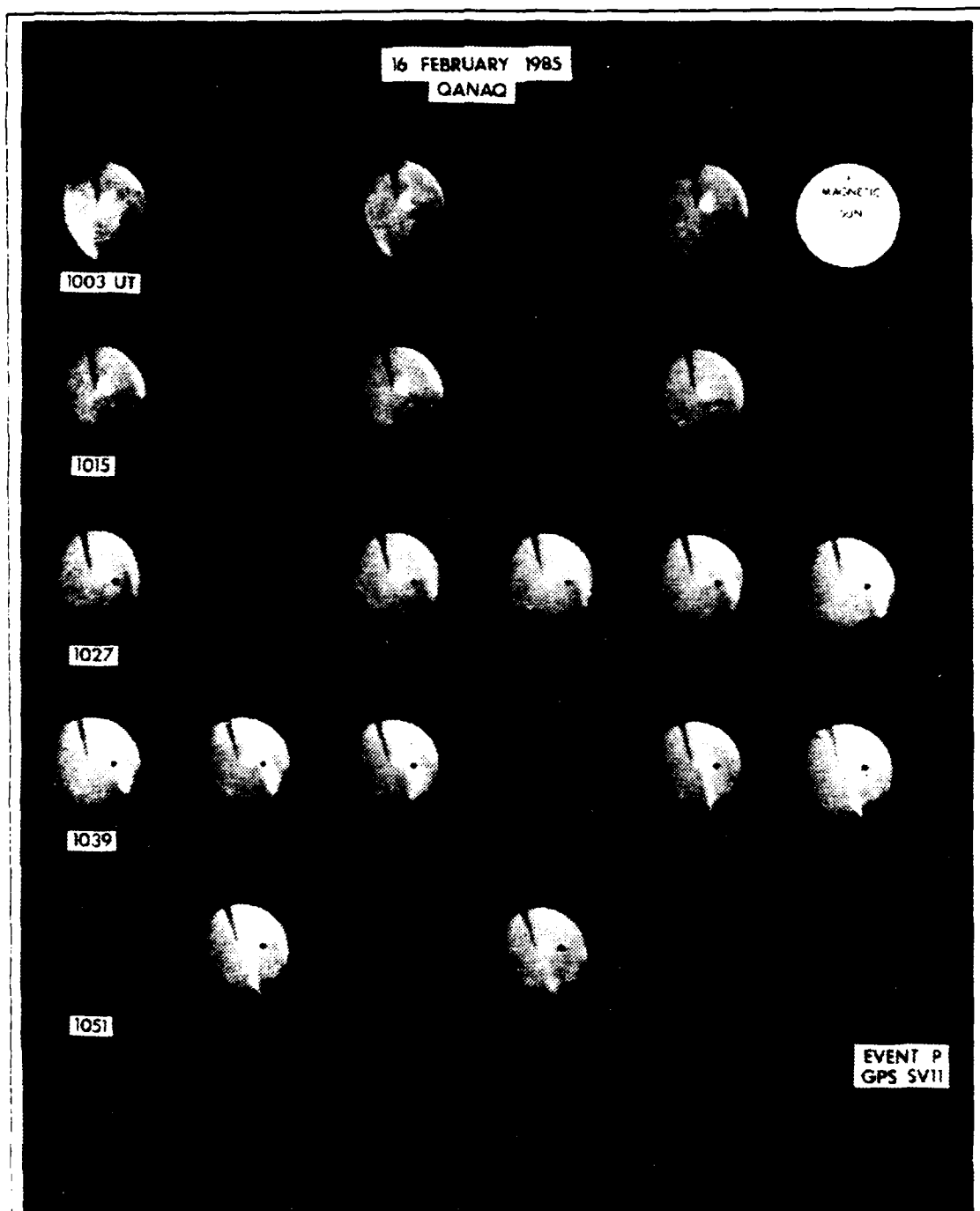
37

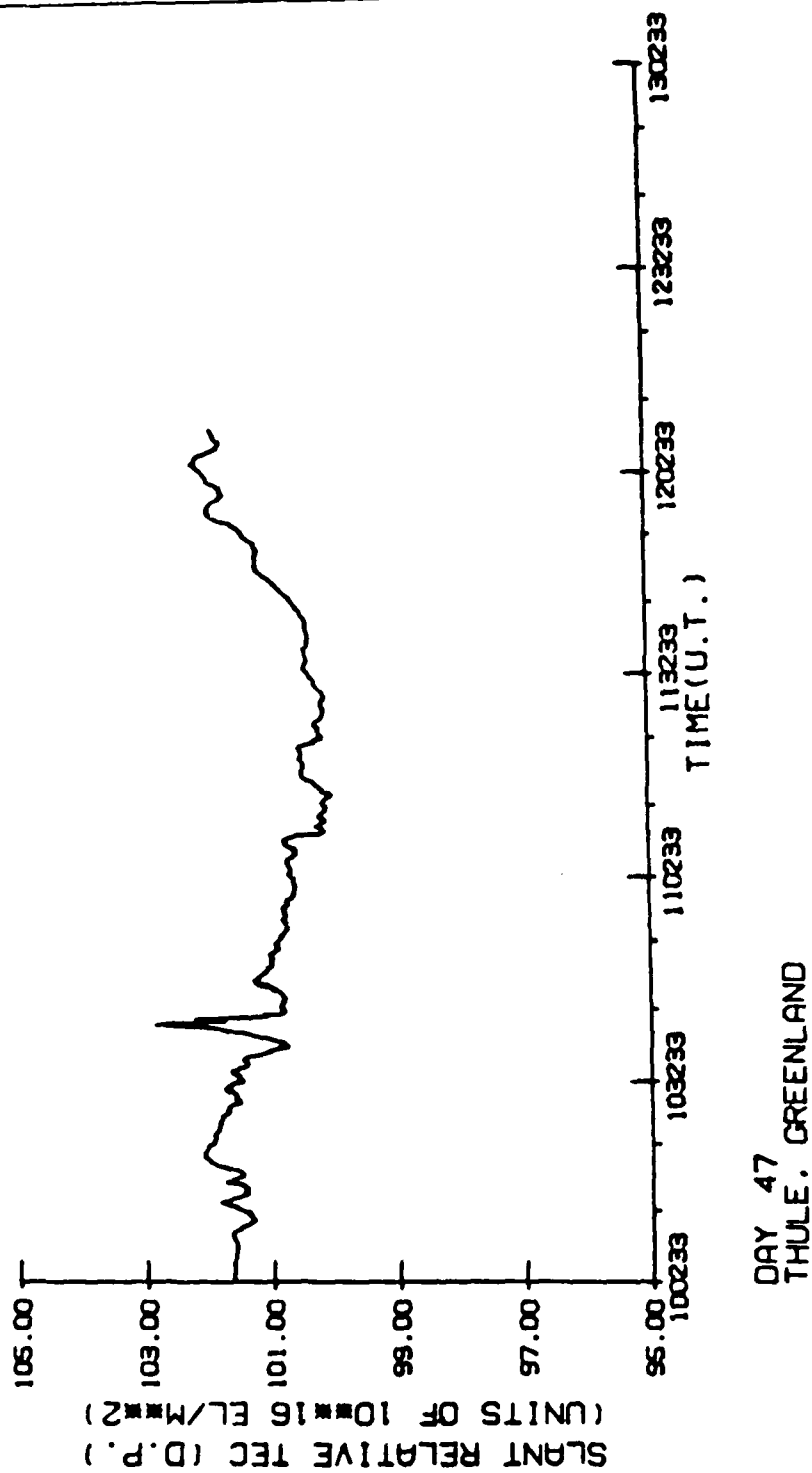Figure 11. ASIP Images: 1003 - 1057 UT, 16 February 1985

38

Figure 12. Relative TEC for 16 February, 1037 - 1053 UT.

39

Although the change in TEC was relatively small, the arc's transit did cause an appreciable change in the $S_4$, an increase from ~0.06 to ~0.12 (Figure 13).

An unusual feature of this arc was that its lifetime in the field of view was as a single arc. In general, the arcs seem to arrive or form parallel to each other in groups, which gives a streaky or striated appearance to the ASIP image. Alternatively, a single arc will divide itself to form two or more separate arcs.

3. Case 3: 25 January and 16 February 1985

There were many instances which exhibited the distinct leading edge but which have highly ambiguous end conditions. These arcs either have no distinguishable trailing edge, or are followed so closely by other arcs or turbulence that they can be classed as one event.

The first example of this began at 2330 UT, 25 January, as indicated the extremely rapid rise in TEC, with a peak increase in level of ~4.7 units. The ASIP image shows a discernable arc moving through the raypath until ~2340 UT, when the primary arc had passed. Almost immediately, however, the images reveal the raypath embedded in a secondary arc which began to form out of the main arc at ~2338 UT (Figure 14). This secondary, which does not eventually form a discernable arc, remained around the
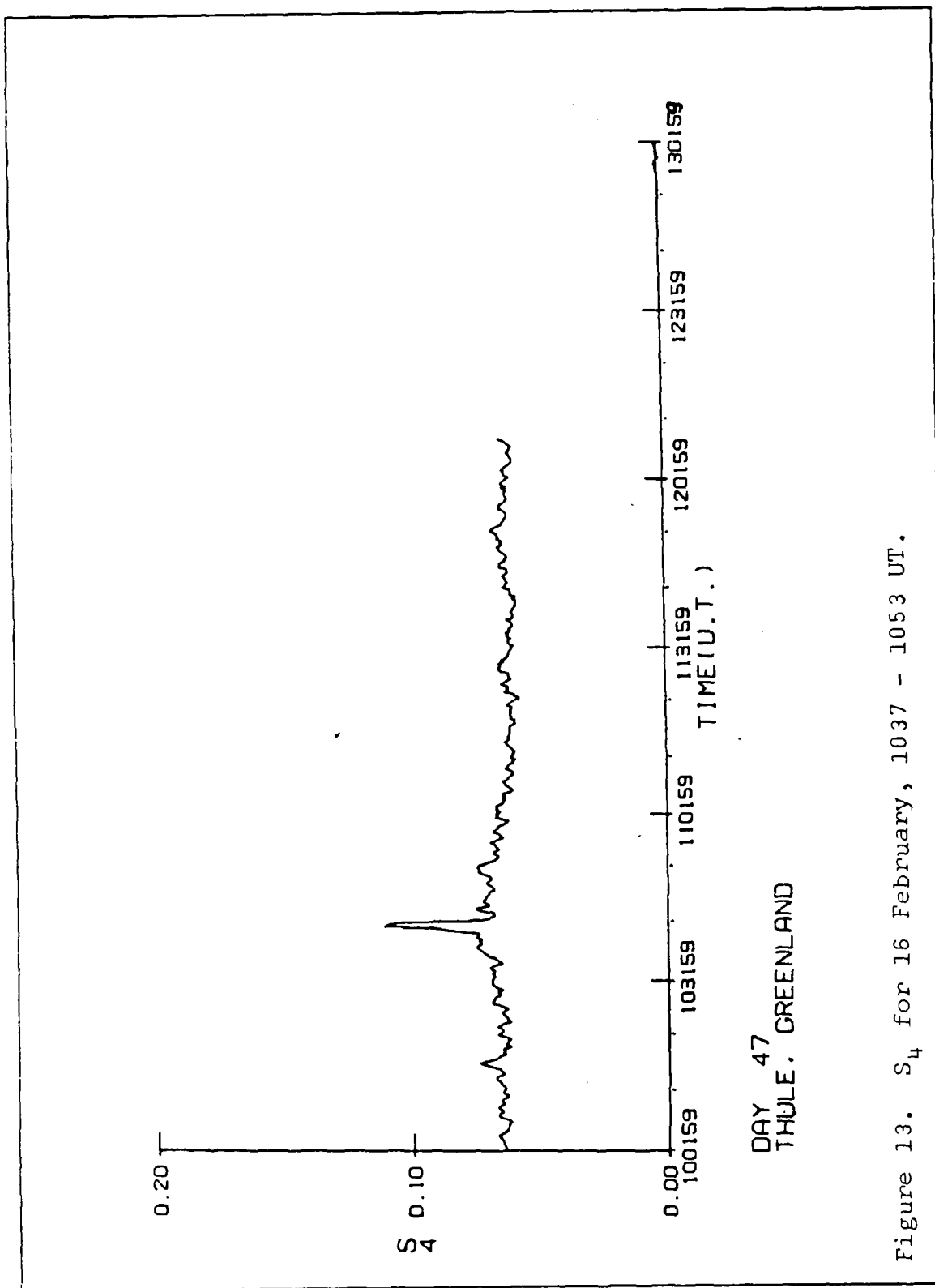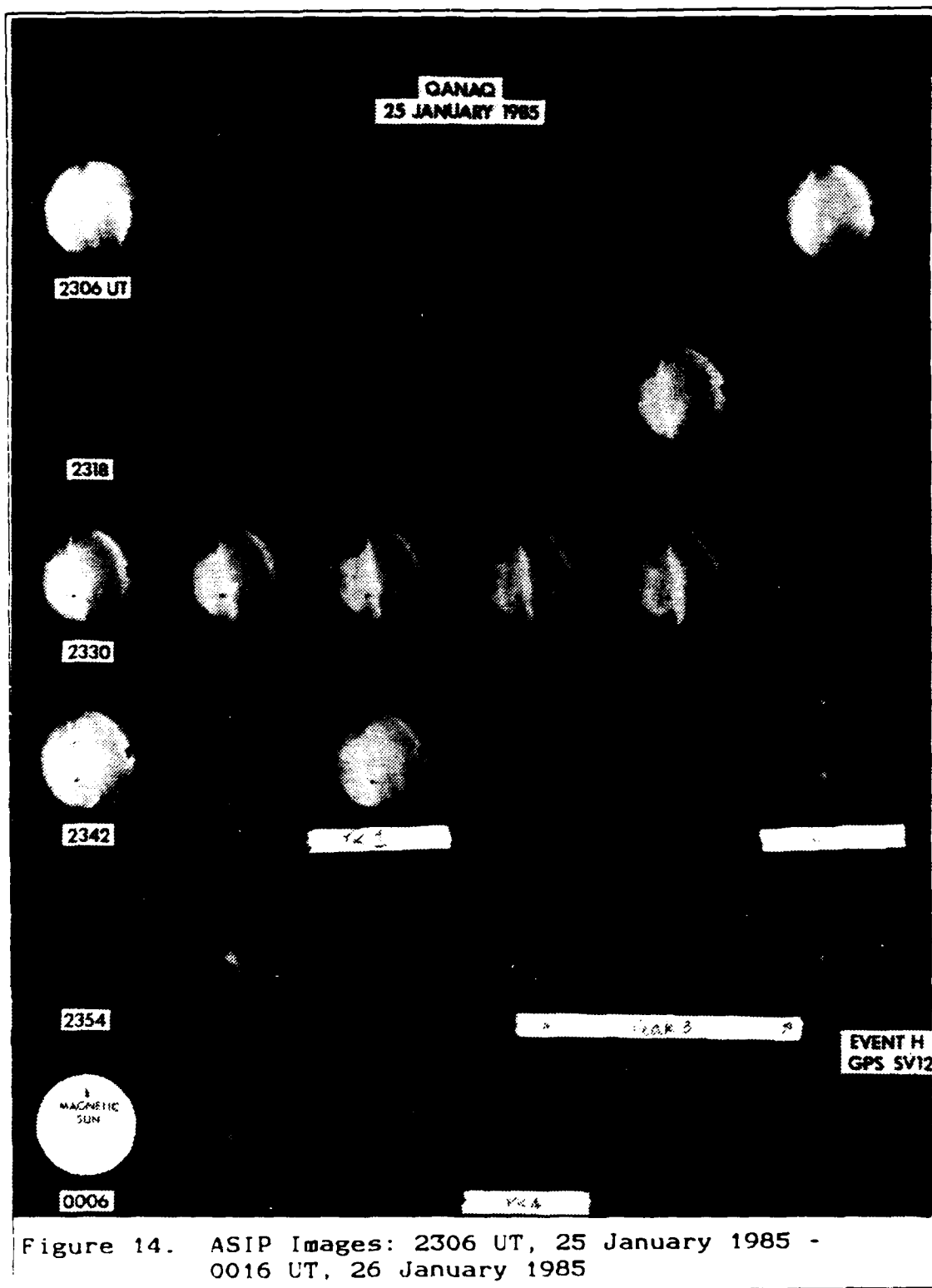
40

Figure 13. $S_4$ for 16 February, 1037 - 1053 UT.

41

Figure 14. ASIP Images: 2306 UT, 25 January 1985 - 0016 UT, 26 January 1985

42

raypath for a number of minutes before moving on, and caused a series of relative enhancements of TEC, with the maximum relative increase at ~5.0 units (Figure 15). The primary arc caused a noticable increase in $S_4$, from ~0.6 to ~0.16, while the disturbed area following it generated an $S_4$ increase of ~0.04 (Figure 16).

A similar but not as severe instance began at 0911 UT on 16 February (Figure 17). The 22 minute transit of the primary arc caused relative TEC enhancements with a maximum value of ~3.8 units. Again, however, the primary arc is closely followed by its own partially formed, split off secondary and an area of generalized turbulence that never successfully coalesces. Although the relative TEC enhancement of the follow-on area is modest, possibly because true minimum was not reached between the arcs, the TEC is increased to a level which is equal to that caused by the primary arc (Figure 18). With the gradual dissipation of the follow-on area, the TEC declined to pre-event levels.

The $S_4$ index for this event was also disturbed (Figure 19). The disturbances were small but still obvious: a 0.03 increase for the primary arc and an increase of ~0.02 for its follow-on area.
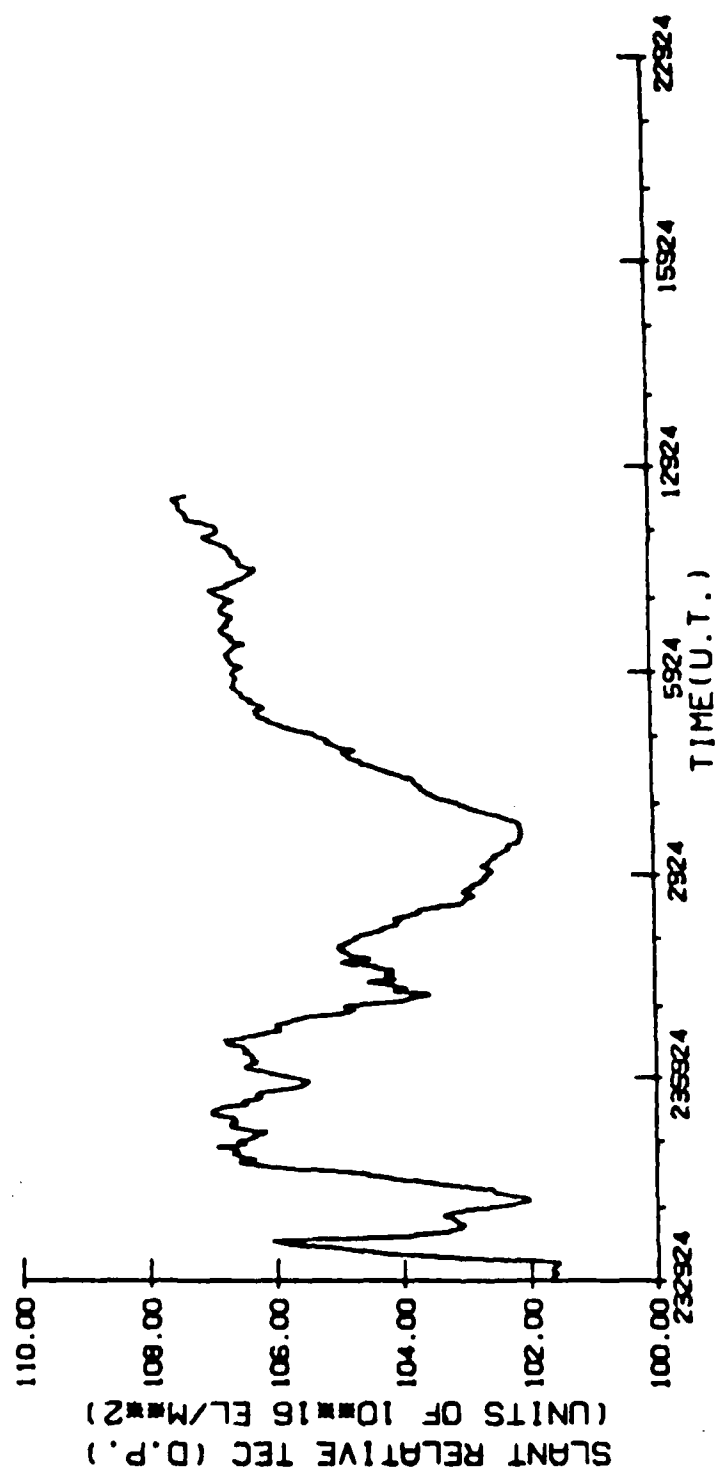
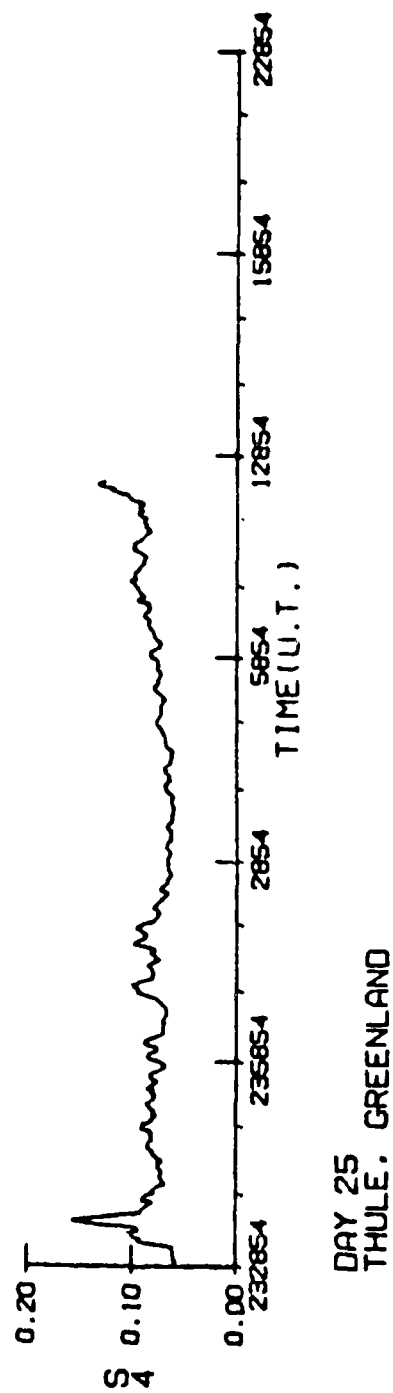Figure 15.    Relative TEC for 25 January, 2330 UT - 26 January, 0016 UT.

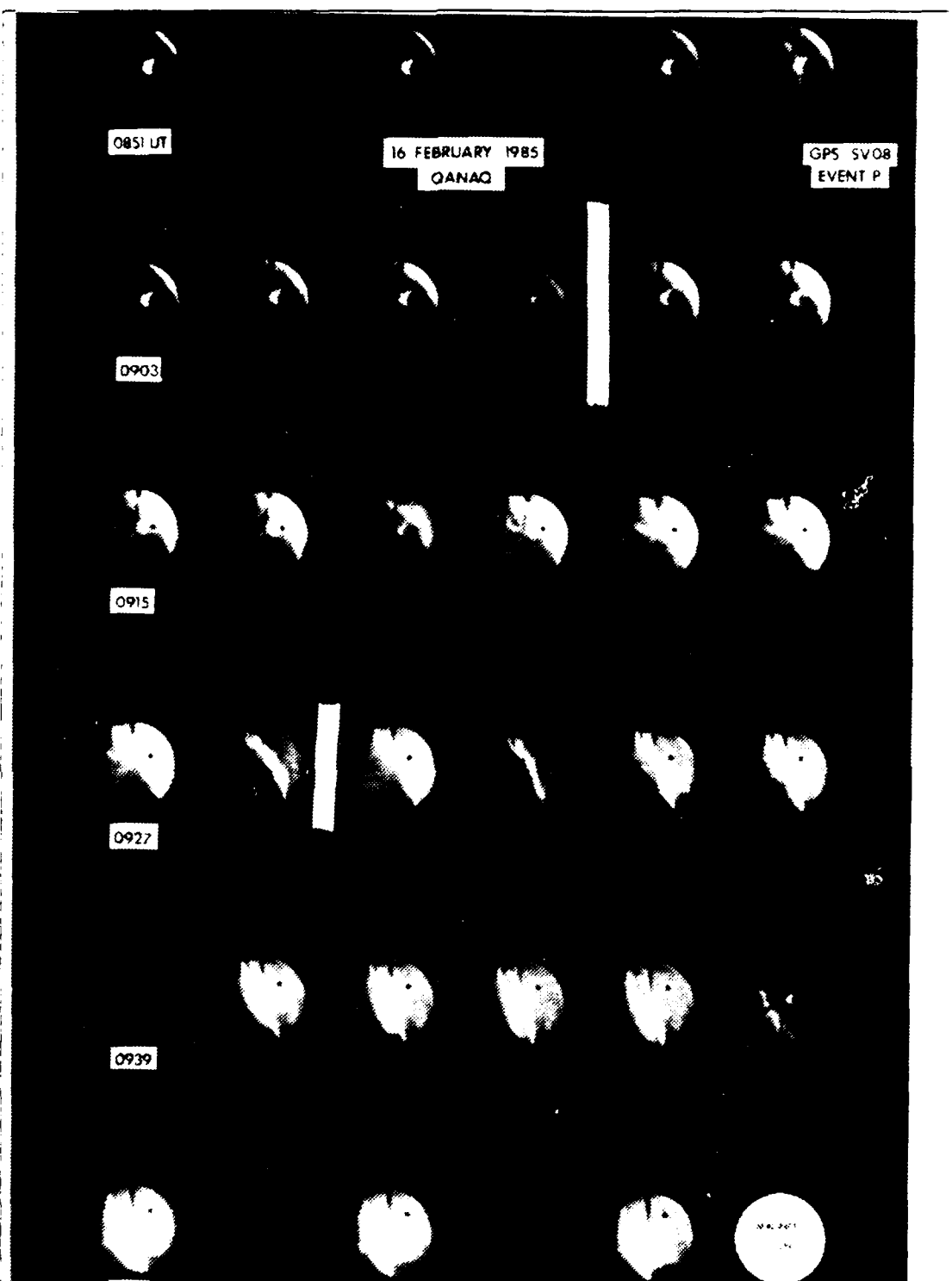Figure 16.  $S_4$  for 25 January, 2330 UT - 26 January, 0016 UT.

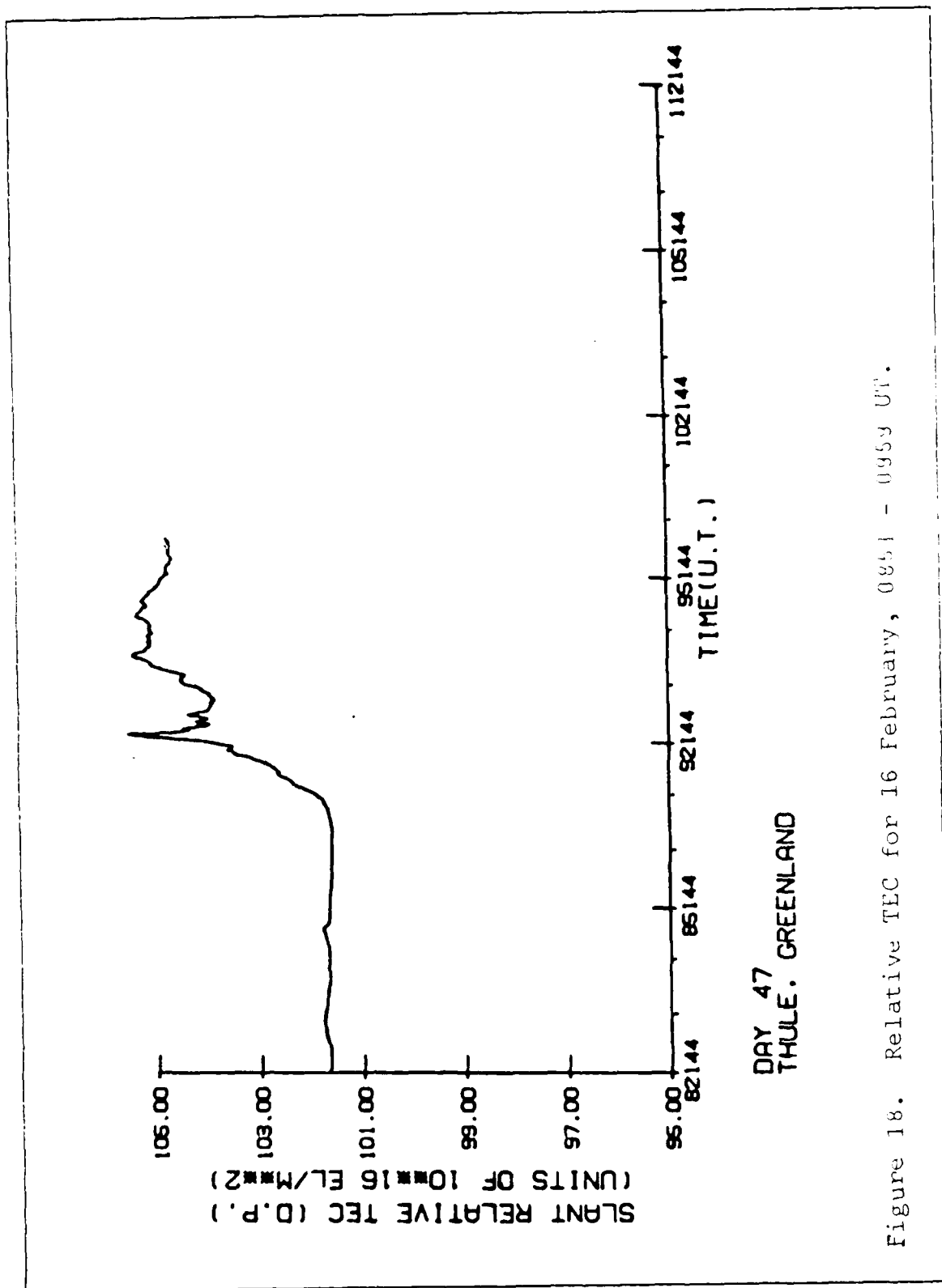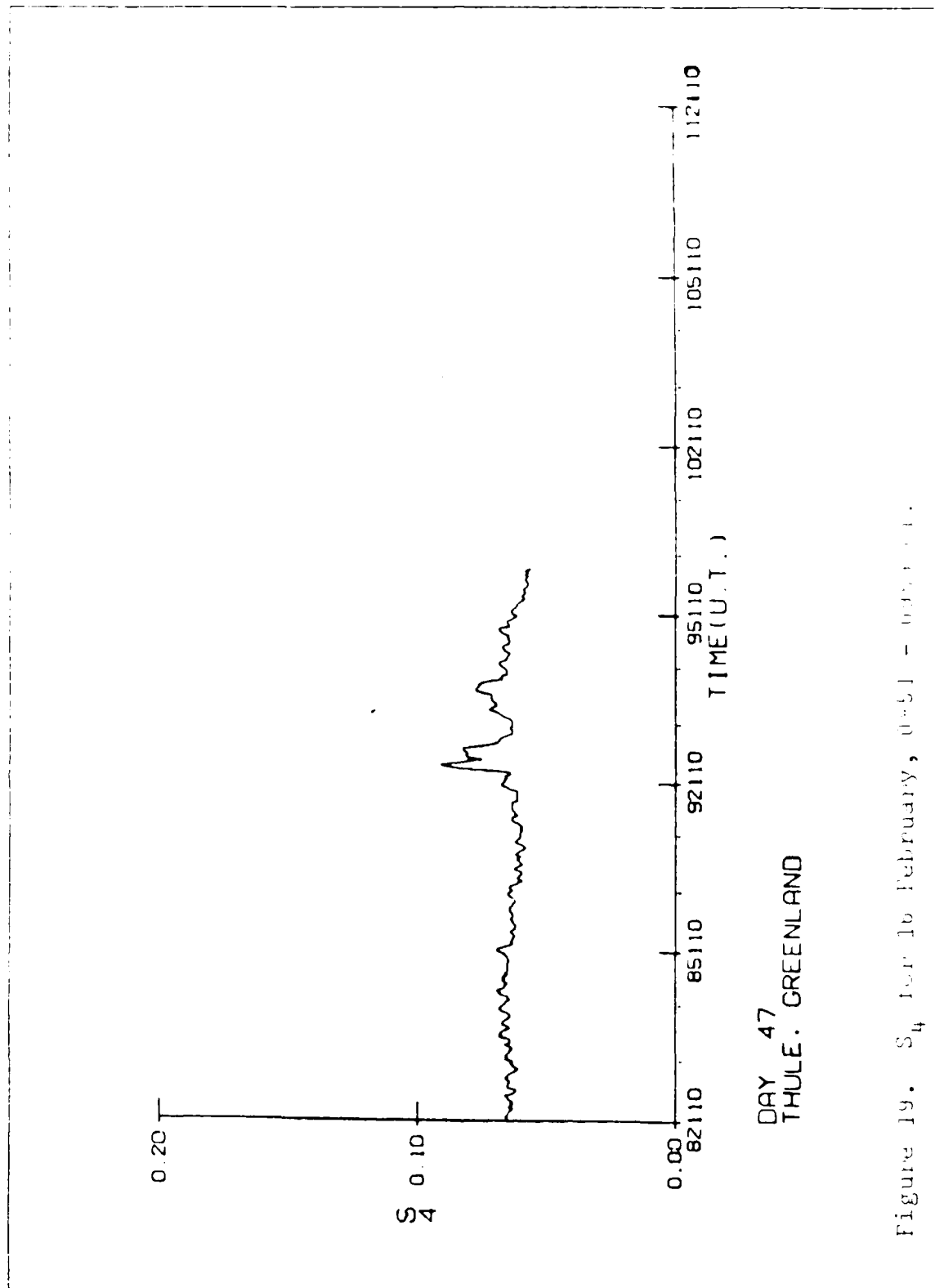Figure 17. ASIP Images: 0851 - 0959 UT, 16 February 1985

46

Figure 18. Relative TEC for 16 February, 0851 - 0959 UT.

Figure 19. $S_4$ for 16 February, 0831 – ...

# IV. DISCUSSION

Arcs and patches are the only structured anomalies to have been discovered in the polar cap. Since the arcs occur when $B_z > 0$, and since $B_z > 0$ conditions exist approximately 50% of the time, the arcs can be said to account for roughly half the irregularity incidences in the polar cap. Therefore, if the arcs are associated with, or indicative of, ionospheric irregularities, their occurrence is a significant factor in calculating and predicting ionospheric effects on $C^3 I$ systems.

Two results seem conclusive from the analysis of data done for this thesis. First, the arcs are clearly associated with large and rapid variation in ambient TEC. Absolute TEC values were not calibrated for the period during which these arc observations were made. However, they were calibrated from GPS code data for a similar observation period a year earlier (January - February 1984), when solar flux was nearly the same. During magnetically quiet periods, the absolute equivalent vertical TEC values were less than 10 x $10'$ $el/m^2$, as shown in Figure 20. Figure 20 (Klobuchar et al., 1986, Figure 3) compares theoretical calculations of polar cap TEC (indicated on the graph by the solid dots), which take into account solar EUV, average polar rain precipitation, and the earth's co-

49

rotation; and actual recorded values of TEC for the quiet day of 1 February 1984. If the absolute TEC values given in Figure 20 are assumed to be approximately the same as for the period January - February 1985, then the observed TEC increases associated with the arcs can be as much as 100%. (Klobuchar et al., 1986; Klobuchar, 1987)



Figure 20. Theoretical (solid dots) and measured absolute equivalent vertical TEC

Second, the arcs also produce small but measurable amplitude scintillation effects even at the comparatively high GPS L2 frequency. The frequency and intensity of ionospheric irregularities increase with sunspot number, so amplitude scintillation effects vary with the level of solar activity. These arcs were observed during a period close to solar minimum (which occurred in 1986); S₄ variations are expected to be much greater in the years approaching solar maximum.

Table 2 is a summary of the TEC and S₄ changes in the arcs discussed.

50

TABLE 2. SUMMARY OF SIGNIFICANT FEATURES.

| CASE | PRIMARY MAX $\Delta$TEC | SECONDARY MAX $\Delta$TEC | PRIMARY $\Delta S_4$ | SECONDARY $\Delta S_4$ |
|------|------|------|------|------|
| 0804 - 0920 26 Jan | 4.4 | --- | --- | --- |
| 1037 - 1053 16 Feb | 2.2 | --- | 0.06 | --- |
| 2330 25 Jan - 0029 26 Jan | 4.7 | 5.4 | 0.10 | 0.04 |
| 0911 - 0959 16 Feb | 3.9 | 1.6 | 0.03 | 0.02 |

Note 1. TEC is in units of $10^{16}$ el/m$^2$.

Note 2. All times are Universal Time (UT).

51

# V. SUMMARY

First-order effects of ionospheric irregularities decrease as frequency increases. Generally, then, HF systems are more likely than L-band systems to experience directly ionospherically induced outages. Even in the VHF range, however, where the majority of U.S. satellite communications frequencies are located, irregularity caused effects, specifically amplitude scintillation, are bad and frequent. Deep signal fades of >20dB are common and well documented (Basu et al., 1986, p.20 and Figure 10). Additionally, as frequencies are increased to accomodate satellite based systems, particularly in communications, flexibility in the system is lost almost completely.

As frequency goes up, the accuracy threshold for minimum acceptable performance is also raised. L-band signals will not be greatly degraded by amplitude scintillation, for example, but the selectivity of the receivers must be so narrow to deliver accurate processed information that even small perturbations may cause a degraded product. A system such as GPS, which advertises extreme accuracy and incorporates self-correction for ionospheric time delay as a basis of the system, is particularly vulnerable to this kind of error.

52

Also susceptible are the space-based radar systems, particularly synthetic aperture radar (SAR). SAR requires a high degree of phase coherence for imaging integrity. The phase coherence of a SAR signal can be easily distorted by phase scintillation effects introduced by irregularities with kilometer range scale sizes, such as those associated with polar cap arcs. The coherency break-up of a SAR signal cannot be easily compensated for, if at all, in the signal processing, since irregularities are neither spatially nor temporally predictable. (Szuszczewicz et al., 1983, pp.766-768)

For the bulk of the $C^3 I$ systems in use or under development, then, the behavior of the F layer is an important--sometimes essential--factor in determining how well those systems perform. With the increasing strategic and tactical importance of the very high latitude areas, the significance of the behavior of polar cap F layer is also increased.

F layer polar cap arcs, which generate enhancements in TEC and measurable amplitude scintillation effects, therefore have the potential for degrading, sometimes seriously, the performance of $C^3 I$ systems operating in or across the polar latitudes.

# LIST OF REFERENCES

Akasofu, S.I., The Polar Caps, National Institute of
    Polar Research (Tokyo) Memoirs of the National
    Institute of Polar Research Special Issue 38, pp.1-
    47, December 1985.

Basu,S., E. MacKenzie, S. Basu, E. Costa, P.F. Fougere,
    H.C. Carlson,Jr. and H.E. Whitney, "250 MHz/Ghz
    Scintillation Parameters in the Equatorial, Polar
    and Auroral Environments", IEEE Transactions on
    Communications, Special Issue on Communications via
    Fading Channels, (pre-print) May 1986.

Burke, W.J., "Magnetosphere-Ionosphere Coupling:
    Contributions from IMS Satellite Observations",
    Reviews of Geophysics and Space Physics, v.20,
    no.3, pp.685-708, August 1982.

Carlson,H.C. Jr., V.B. Wickwar, E.J. Weber, J. Buchau,
    J.G. Moore and W. Whiting, "Plasma Characteristics
    of Polar Cap Arcs", Geophysical Research Letters,
    v.1, no.9, pp.895-898, September 1984.

Chamberlain, Joseph W., Theory of Planetary Atmospheres
    - An Introduction to Their Physics and Chemistry,
    pp.163-195, Academic Press, 1978.

Cretcher, C.K., "Ionospheric Effects in NAVSTAR-GPS", In
    Effects of the Ionosphere on Space Systems and
    Communications, ed. J.M. Goodman, Naval Research
    Laboratory, Washington, D.C.: U.S. Government
    Printing Office, pp.403-410, 1975.

Demaro, R.P., "The All-Purpose Satellite", IEEE
    Spectrum, v.18, no.5, pp.35-40, May 1981.

Doherty, P.H., Physics Research Division, Emmanuel
    College, Boston, Massachusetts, private
    communication, June 1987.

Eliasson,L., R. Lundin and J.S. Murphree, "Polar Cap
    Arcs Observed by the Viking Satellite", Geophysical
    Research Letters, v.14, no.4, pp.451-454, April
    1987.

Gnanalingam, S., PH 4515 class notes, Naval Postgraduate
    School, Monterey, California, July 1987.

Gussenhoven,M.S., "Extremely High Latitude Aurora", *Journal of Geophysical Research*, v.87, no.A4, pp.2401-2412, April 1982.

Hardy,D.A., "Intense Fluxes of Low-Energy Electrons in Geomagnetic Latitudes above 85°", *Journal of Geophysical Research*, v.89, no.A6, pp.3883-3892, June 1984.

Heelis,R.A., "The Polar Ionosphere", *Reviews of Geophysics and Space Physics*, v.20, no.3, pp.567-576, August 1982.

Klobuchar,J.A., *Ionospheric Effects on Earth-Space Propagation*, Air Force Geophysics Laboratory Environmental Research Paper 866 (AFGL-TR-84-0004), pp.1-18, 27 December 1983.

Klobuchar,J.A., G.J. Bishop, and P.H. Doherty, "Total Electron Content and L-Band Amplitude and Phase Scintillation Measurements in the Polar Cap Ionosphere", Presented at AGARD Symposium on Propagation Effects on Military Systems in the High Latitude Region, Fairbanks, AK, 3-7 June 1985.

Klobuchar,J.A., D.N. Anderson, G.J. Bishop, and P.H. Doherty,"Measurement of Trans-Ionospheric Propagation Parameters in the Polar Cap Ionosphere", Presented at the International Beacon Satellite Symposium on Radio Beacon Contribution to the Study of Ionization and Dynamics of the Ionosphere and to Corrections to Geodesy, Oulu, Finland, June 1986.

Klobuchar, J.A., Ionospheric Physics Division, Air Force Geophysics Laboratory, Hanscom AFB, Massachussetts, private communication, August 1987.

Szuszczewicz, E.P., *The Unique Arctic Environment, Associated Effects on Naval C3I Operations and Implications for Future Space Systems*, Naval Research Laboratory Memorandum Report 5293, pp.1-16, 28 March 1984.

Szuszczewicz,E.P., P.Rodriguez, M. Singh, and S. Mango, "Ionospheric Irregularities and Their Potential Impact on Synthetic Aperture Radar", *Radio Science*, v.18, no.5, pp. 765-774, September - October 1983.

55

Weber,E.J., J. Buchau, R.H. Eather and J.W.F. Lloyd, Large Scale Optical Mapping of the Ionosphere, Air Force Geophysics Laboratory Environmental Research Paper 611 (AFGL-TR-77-0236), pp.7-11, 21 October 1977.

Weber,E.J., and J. Buchau, "Polar Cap F-Layer Auroras", Geophysical Research Letters, v.8, no.1, pp.125-128, January 1981.

Weber,E.J., J. Buchau, J.G. Moore, J.R. Sharber, R.C. Livingston, J.D. Winningham, and B.W. Reinisch, "F-Layer Ionization Patches in the Polar Cap", Journal of Geophysical Research, v.89, no.A3, pp.1683-1694, 1 March 1984.

Weber,E.J:, J.A. Klobuchar, J. Buchau, H.C. Carlson,Jr., R.C. Livingston, O. De la Beaujardiere, M. Mcready, J.G. Moore and J.G. Bishop, "Polar Cap F-Layer Patches: Structure and Dynamics", Journal of Geophysical Research, v.91, no.A11, pp.12121-12129, 1 November 1986

Yeh,K.C., and C.H. Liu, "Radio Wave Scintillation in the Ionosphere", Proceedings of the IEEE, v.70, no.4,p.324, April 1982.

# INITIAL DISTRIBUTION LIST

No. copies

1.  Commander                                              2
    Naval Space Command
    Attn: Code N3
    Dahlgren, VA   22448

2.  Defense Technical Information Center                   2
    Cameron Station
    Alexandria, VA   22304-6145

3.  Commander                                              2
    United States Space Command
    Attn: Technical Library
    Peterson AFB, CO   80914

4.  Library, Code 0142                                     2
    Naval Postgraduate School
    Monterey, CA   93943-5002

5.  Superintendent                                         1
    Naval Postgraduate School
    Attn: Adj. Prof. S. Gnanalingam Code 61Gm
    Monterey, CA  93943-5000

6.  Commander                                              2
    Air Force Geophysics Laboratory
    Attn: LIS/Dr. E.J. Weber
    Hanscom AFB, MA 01731

7.  LT. D.D. Fite                                          2
    General Delivery
    P.O. Box 1000
    Peterson AFB, CO 80914

# END

# DATE

# FILM

# JAN

# 1988